exon 11b (ε-SG8$^+$/11b$^-$), while another 377-bp fragment was a novel transcript containing exon 11b, but lacking exon 8 (ε-SG 8$^-$/11b$^+$).

3.2. Identification of protein products from ε-SG transcripts

We generated three antibodies, Esg-C1, Esg-C2, and Esg-E8, that recognize variant-specific C-terminal structures

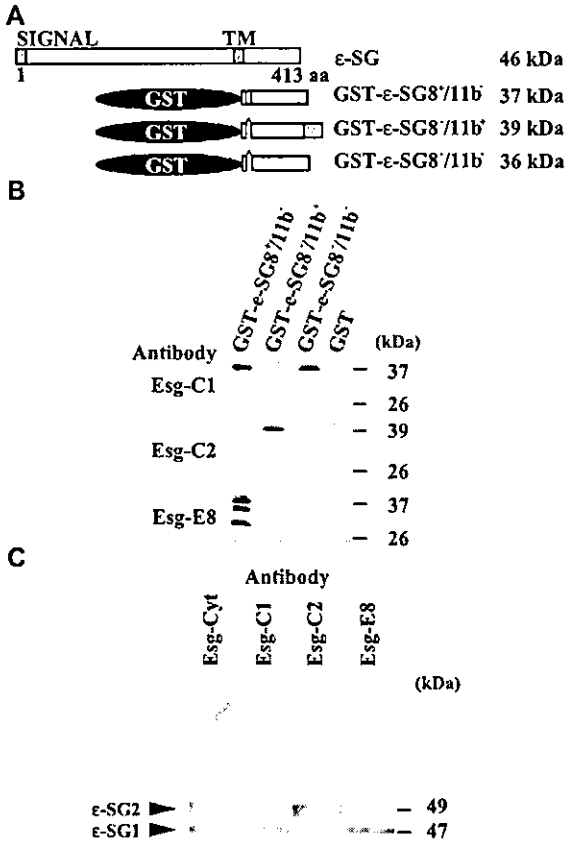

Fig. 3. Identification of protein products of ε-SG transcript variants in the mouse brain. (A) Schematic representation of GST-ε-SG fusion proteins that were used for testing immunoreactivities of antibodies, Esg-C1, Esg-C2, and Esg-E8. The shaded boxes in the N-terminal of ε-SG8$^+$/11b$^-$ and the C-terminal of ε-SG8$^-$/11b$^+$ indicate the peptide structures produced by the inclusion of exon 8 and exon 11b, respectively. (B) Specific reactivities of Esg-C1, Esg-C2, and Esg-E8 antibodies to ε-SG variants. Immunoblotting of GST-ε-SG-fusion proteins showed that Esg-C1 and Esg-C2 antibodies recognize the C-terminal of ε-SG excluding and including exon 11b, respectively. Esg-E8 was shown to recognize the ε-SG inclusion of exon 8. Note that Esg-E8 antibody recognizes degradation products of GST-ε-SG8$^+$/11b$^-$ protein. (C) Expression of two ε-SG isoforms in adult mouse brain. Ten micrograms of tissue lysate were separated on SDS-PAGE (9% polyacrylamide gel) and transferred onto polyvinylidene difluoride (PVDF) membranes. The membranes were sequentially treated with affinity-purified rabbit antibodies, Esg-C1, Esg-C2, and Esg-E8, and a horseradish peroxidase (HRP)-conjugated anti-rabbit secondary antibody. Immunostained bands were detected using a chemiluminescence detection system. The staining pattern of the antibody against the whole cytoplasmic region of ε-SG is shown in the left lane as Esg-Cyt.

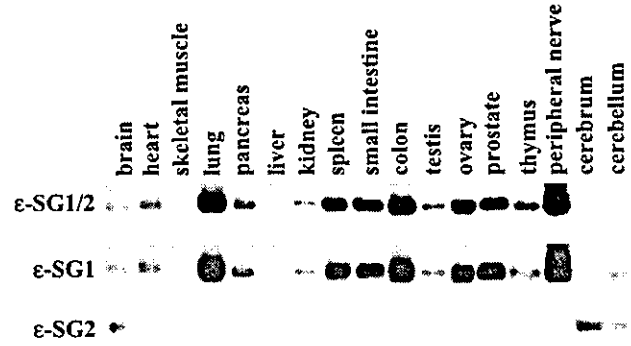

Fig. 4. Tissue expression of ε-SG1 and ε-SG2. Expression of the two ε-SG isoforms, ε-SG1 and ε-SG2, was examined in fifteen mouse tissues by immunoblotting. Ten micrograms of tissue lysates were separated on 9% SDS-PAGE and stained with the antibodies Esg-C1 and Esg-C2. The upper panel, indicated as ε-SG1/2, shows the staining pattern with Esg-Cyt antibody.

of ε-SG. Esg-C1 recognizes the C-terminal of ε-SG, which is the product of transcripts including exon 12, but lacking exon 11b. Esg-C2 recognizes the C-terminal of the other ε-SG, which is the product of transcripts including exon 11b and 12. Esg-E8 recognizes ε-SG, corresponding to transcripts that include exon 8 (Fig. 3B).

Immunoblotting of the mouse brain lysate with an antibody against the whole cytoplasmic region, Esg-Cyt, showed 47 and 49 kDa bands (Fig. 3C). Esg-C1 and Esg-E8 antibodies reacted to the 47 kDa band but not the 49 kDa, while Esg-C2 antibody reacted to the 49 kDa band but not the 47 kDa. These results indicated that two ε-SG isoforms are expressed mainly in the mouse brain. One is a conven-

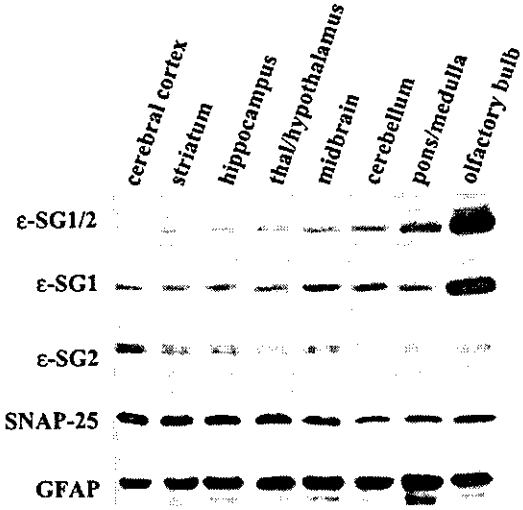

Fig. 5. Regional distribution of ε-SG1 and ε-SG2 in adult mouse brain. Adult mouse brains were separated into eight regions and homogenized in lysis buffer. These lysates were separated by SDS-PAGE (9% polyacrylamide gel) and immunostained with the antibodies Esg-C1 and Esg-C2. The upper panel (ε-SG1/2) shows the staining pattern with the Esg-Cyt antibody. The panels indicated as SNAP-25 and GFAP show the relative amounts of neuronal cells and astrocytes in each brain region. The thal/hypothalamus and pons/medulla indicate the regions including the thalamus and hypothalamus, and pons and medulla oblongata, respectively.

tional 47 kDa isoform derived from a transcript encoding exon 12 but not exon 11b, another is a novel 49 kDa isoform derived from a transcript encoding exon 11b, but not exon 8. We designated the former ε-SG1 and the latter ε-SG2.

The analysis of tissue expression with Esg-C1 and Esg-C2 antibodies showed that ε-SG1 was widely expressed in a variety of tissues, including brain, heart, skeletal muscle, lung, pancreas, liver, kidney, spleen, small intestine, colon, testis, ovary, prostate, thymus, peripheral nerve, while ε-SG2 was detected only in brain (Fig. 4).

3.3. Regional distribution of ε-SG1 and ε-SG2 in the mouse brain

We further examined the expression of the ε-SGs in eight regions of the mouse brain. Immunoblotting with Esg-C1 and Esg-C2 antibodies detected ε-SG1 and ε-SG2 in all regions examined: the cerebral cortex, striatum, hippocampus, thalamus/hypothalamus, midbrain, cerebellum, pons/medulla oblongata, and olfactory bulb (Fig. 5). The expression of ε-SG1 was more prominent in the olfactory bulb, while the expression of ε-SG2 was less abundant in the cerebellum, pons/medulla oblongata, and olfactory bulb.

3.4. Localization of ε-SG in the mouse brain

To identify the localization of ε-SGs, we performed immunocytochemical studies with the Esg-Cyt antibody. ε-SG immunoreactivity was clearly observed throughout the brain, but its signal is relatively high in olfactory bulb, cerebral cortex, hippocampus, pons, and cerebellar cortex (Fig. 6A). The ε-SG immunoreactivity partially overlapped

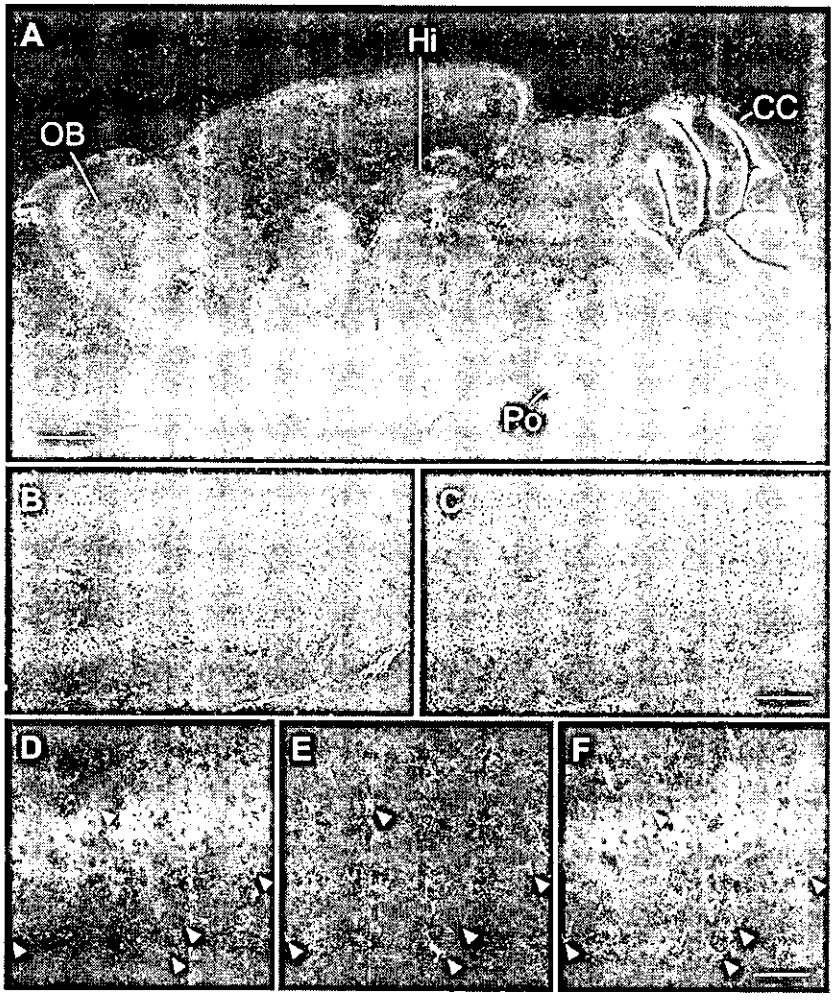

Fig. 6. Distribution of ε-SGs in adult mouse brain. Parasagittal cryosections of adult mouse brain were reacted with the Esg-Cyt antibody. The ε-SG immunoreactivity was visualized using Alexa488-conjugated secondary antibody (green). (A) Immunoreactivity of ε-SGs in a whole parasagittal section of mouse brain. The signals in the olfactory bulb (OB), hippocampus (Hi), pons (Po), and cerebellar cortex (CC) were intense. (B) and (C) Indicate the double-stain patterns of the dentate gyrus with Esg-Cyt rabbit antibody (green) and anti-lamini-α2 chain rat antibody (red) or Cy3-conjugated anti-GFAP mouse antibody (red), respectively. Note that the red fluorescence of lamini-α2 signals are seen as orange or yellow because of colocalization with the green signal of ε-SGs. (D–F) Higher magnification of a hippocampal CA2 region that was double-stained with Esg-Cyt (D) and Cy3-anti-GFAP antibody (E), and their merged image (F). Arrowheads indicate astrocytes showing immunoreactivity of ε-SGs. Scale bar = 1 mm for A, 100 μm for B and C, 50 μm for D–F. (For interpretation of the references to colour in this figure legend, the reader is referred to the web version of this article.)

with capillary vasculature stained with an antibody against laminin-α2 chain, a component of basal lamina surrounding micro-capillaries (Fig. 6B), whereas the localization of ε-SG was different from that of GFAP, a marker of astrocytes (Fig. 6C). In a higher magnification, however, a faint signal was detected in some astrocytes (Fig. 6D–F). Double-staining analysis with the Esg-Cyt antibody and fluorescent Nissl stain showed that ε-SGs expressed in neuronal cells within the olfactory bulb, hippocampus, pons, and cerebellar cortex, and localized along their cell bodies (Fig. 7). Furthermore, ε-SG immunoreactivity was detected in the cells expressing tyrosine hydroxylase (TH) within the sub-

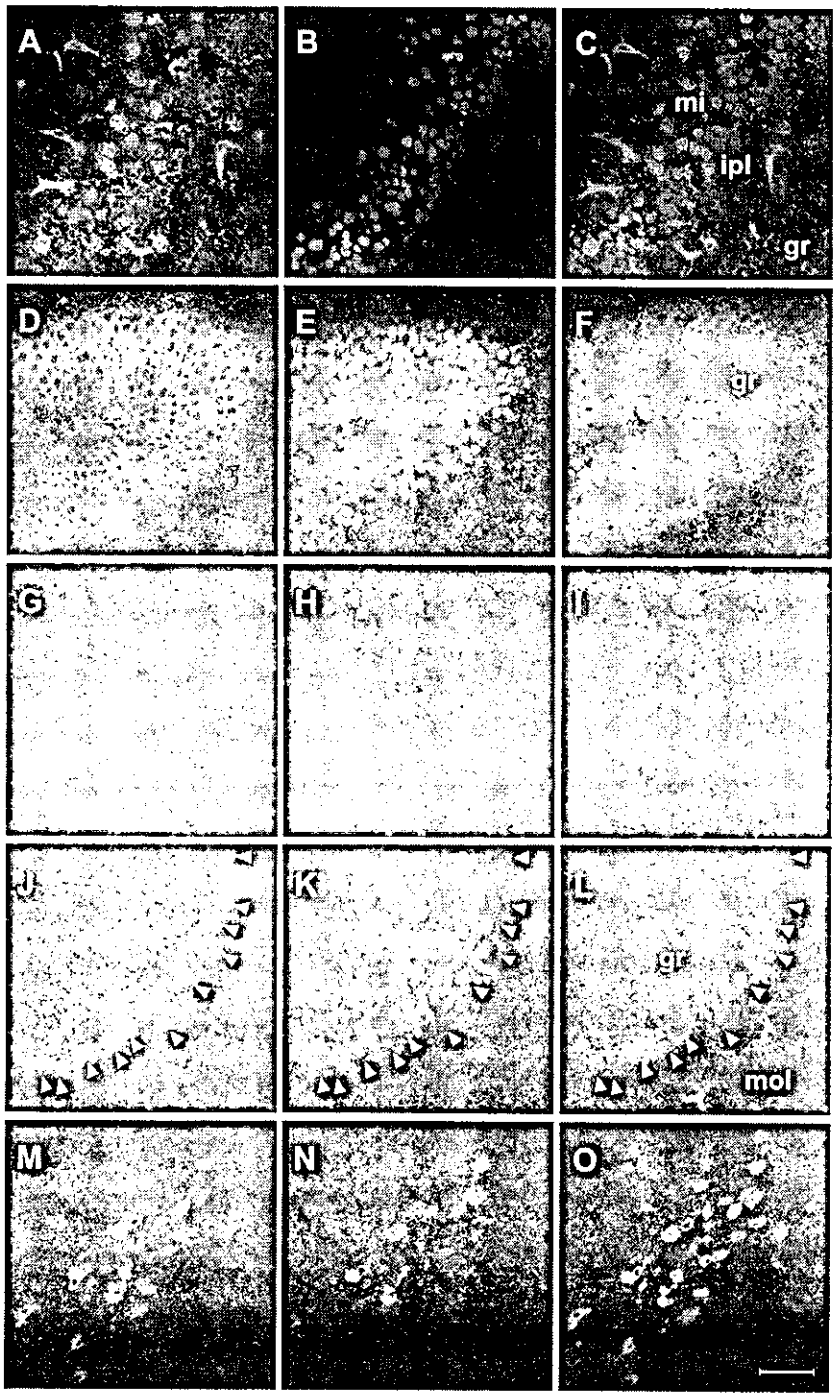

Fig. 7. Localization of ε-SGs in neuronal cells. Double-staining of mouse brain cryosections using Esg-Cyt antibody (A, D, G, J, M) and NeuroTrace™ fluorescent Nissl stain (B, E, H, K) was performed. The figures focus on the regions of the olfactory bulb (A–C), dentate gyrus (D–F), pons (G–I), and cerebellar cortex (J–L). In the staining of the substantia nigra (M–O), anti-TH sheep antibody was used instead of fluorescent Nissl stain and visualized by an Alexa568-secondary antibody (N). All the right-hand panels (C, F, I, L, O) are merged images of the two preceding panels. Arrowheads in panels J–L indicate Purkinje cells. mi, mitral cell layer; ipl, internal plexiform layer; gr, granular cell layer; mol, molecular cell layer. Scale bar = 50 μm.

stantia nigra, indicating that ε-SG is expressed in dopaminergic neurons (Fig. 7M–O). Neither Esg-C1 nor Esg-C2 antibody was available for immunocytochemical study.

3.5. Subcellular localization of ε-SG isoforms in the mouse brain

We examined the expression pattern of ε-SG1 and ε-SG2 in various subcellular compartments of mouse brain to elucidate their roles in the central nervous system.

Fig. 8 shows the brain subcellular fractions prepared according to the procedure of Huttner et al. [18]. We first examined the distribution of several neural membrane markers, such as a marker for synaptic vesicles, synaptophysin; one for pre-synaptic membranes, SNAP-25; and one for post-synaptic membranes, PSD-95. Synaptophysin was remarkably enriched in the LP2 fraction but not in LP1 and PSD fractions, whereas PSD-95 was enriched in LP1 and PSD fractions but not in the LP2 fraction. These results were consistent with previous reports [12]. On the other hand, SNAP-25 was found in LP1 as well as the LP2 fraction, but not found in the PSD fraction. We then examined the expression of ε-SG1 and ε-SG2. ε-SG1 was mainly present in P2 and P3 fractions, but more concentrated in LP1 than in the LP2 fraction. ε-SG2 was also concentrated in P2 and P3 fractions, but distributed equally in LP1 and LP2 fractions. Neither isoform was enriched but certainly existed in the PSD fraction.

We further analyzed the expression of ε-SG isoforms in the brain capillary endothelial cell fraction purified with BS-1 lectin beads [9] (Fig. 8C). In the isolated endothelial cells, we were able to rule out the expression of a neuronal marker

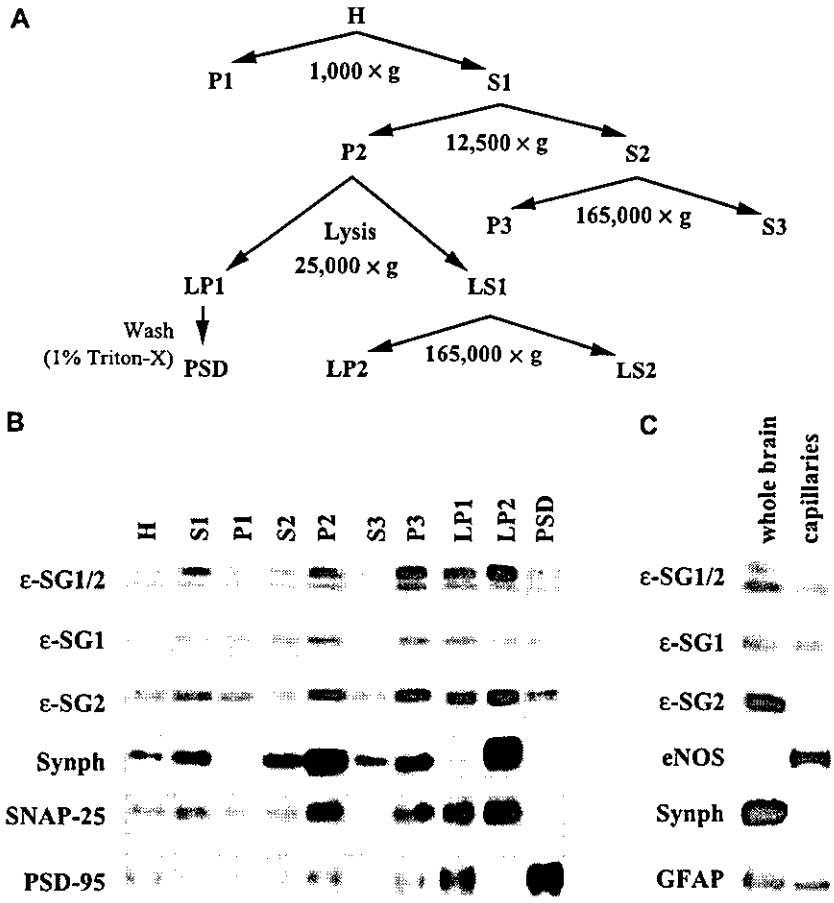

Fig. 8. Subcellular localization of ε-SG1 and ε-SG2 in adult mouse brain. (A) Schematic of the biochemical fractionation. The subcellular fractionation of mouse brain was carried out according to the procedure of Huttner et al. [18]. Fractions are as follows: H, total brain homogenates; P1, nuclei and large debris; P2, a crude synaptosomal fraction; P3, a light membrane/microsome-enriched fraction; LP1, a synaptosomal membrane fraction; LP2, a synaptic vesicle-enriched fraction. Each of the supernatants is designated S1, S2, or S3. A post-synaptic density fraction (PSD) was prepared from LP1 according to the method of Phillips et al [44]. (B) Detection of ε-SG isoforms in subcellular fractions from adult mouse brain. The isolated biochemical fractions were separated by SDS-PAGE (9% polyacrylamide gel) and then blotted with the antibodies, Esg-C1 (ε-SG1), Esg-C2 (ε-SG2), or Esg-Cyt (ε-SG1/2). Subcellular compartments were identified by detection of resident marker proteins with the corresponding antibodies. These markers are synaptophysin (Synph) for synaptic vesicles, SNAP-25 for pre-synaptic membranes, and PSD-95 for post-synaptic membranes. (C) Detection of ε-SG1 in brain capillaries. The capillary endothelial cells were isolated from the mouse brain by BS-1 lectin-beads [9], and the expression of ε-SG1 and ε-SG2 in the cells was analyzed by immunoblotting. Ten micrograms of proteins of mouse whole brain and the isolated capillaries were used for the analysis. eNOS, endothelial nitric oxide synthase, is a marker for endothelial cells.

(synaptophysin), but did detect an astrocyte marker (GFAP), indicating a close association of astrocytes with capillary endothelial cells. Immunoblotting using Esg-C1 and Esg-C2 antibodies clearly found ε-SG1, but not ε-SG2, in the cells. This result revealed that ε-SG1 is predominantly expressed in capillary endothelial cells and astrocytes.

4. Discussion

Mutations in the *ε-SG* gene (*SGCE*) cause M-D, indicating the functional importance of ε-SG in the central nervous system [51]. Despite much work on *SGCE* mutations in M-D families, very little is known about the localization and function of the protein product of *SGCE* in the central nervous system. In the present study, we found two isoforms of ε-SG in the mouse brain and investigated their distribution and localization.

We have shown the expression of two ε-SG isoforms in the mouse brain. One is identical to the ε-SG (ε-SG8$^+$/11b$^-$) that was initially discovered by cDNA cloning of mouse lung [14], and the other is a novel isoform excluding exon 8 and including exon 11b (ε-SG8$^-$/11b$^+$). We propose to designate the former ε-SG1 and the latter ε-SG2. The same results were obtained from human brain on mRNA and protein levels. In addition, ε-SG8$^-$/11b$^-$ type transcripts were markedly expressed in human brain (data not shown). This finding suggested that ε-SG2 plays some specific role in the mammalian brain.

Previous immunocytochemical studies showed ε-SG expression in a variety of cell types, i.e., striated and smooth muscles, capillary blood vessels, Schwann cells in peripheral nerves, alveoli and bronchioles in lung, and glomerular mesangium in kidney [14,20]. The present study showed that ε-SGs are widely distributed throughout the brain and that they are expressed in neuronal and non-neuronal cells including capillary endothelial cells and astrocytes. Immunolabeling of whole mouse brain sections revealed that the ε-SG expression was most marked in the neuronal cells within the olfactory bulb, hippocampus, cerebral cortex, pons, and cerebellar cortex. In almost all cases, ε-SG around cell bodies was more remarkable than that of fibrous structures.

Subcellular fractionation of brain homogenate suggested differential localization of ε-SG1 and ε-SG2 in synaptosomal membranes. We speculate that the two ε-SG isoforms, ε-SG1 and ε-SG2, play different roles at synapses in neurons, and this difference may relate to the structural difference of ε-SGs at their cytoplasmic domains (Fig. 1). Sequence analysis of this domain using the BLAST program (blastp) did not suggest any candidate gene, but a consensus sequence (Arg-Lys-Leu-Thr) for a phosphorylation site of cAMP- and cGMP-dependent protein kinase is present in the ε-SG2 C-terminal. To clarify the roles of ε-SG isoforms in the brain, it is important to search out proteins that interact with their unique cytoplasmic domains.

SGs (α, β, γ, and δ) are thought to function only when they form a subcomplex (SGC) within the dystrophin-DAP complex. ε-SG1 also has been shown to participate in forming SGCs in the smooth muscle and peripheral nervous system [20,47]. Therefore, the question arises whether the ε-SGs play a role as a constituent of the DAP complex that anchors dystrophin in the central nervous system or not. Several different promoters, scattered throughout the *dystrophin* gene, drive the tissue-specific expression of full-length dystrophins (427 kDa) and various short dystrophin isofroms including dystroglycan-binding sites, i.e., Dp260, Dp140, Dp116, and Dp71, in reference to their respective molecular sizes [5,11,17,27,30,35]. Among these dystrophins, full-length dystrophin (Dp427), Dp140, and Dp71 are expressed in the central nervous system. Dp427 is found almost exclusively in neurons in the cerebral cortex and cerebellar cortex, and localized along the plasma membrane of their perikaryons and the proximal dendrites [29,37]. It is also expressed in the hippocampal pyramidal cell layer but not in granule cells of the dentate gyrus. Within the cerebellar cortex, Dp427 is found in Purkinje cells but not in granule cells, Golgi cells, and basket cells. On the other hand, Dp140 is found in astrocytic processes throughout the neuropil, along penetrating microvasculature, and on the cells ensheathing olfactory neurons [30]. The major dystrophin isoform in the brain, Dp71, is expressed in the cerebral cortex, granule cells of the hippocampal dentate gyrus, olfactory bulb, and pituitary gland [34]. These brain dystrophins have been shown to form several types of complex with some dystrophin-accociated proteins, i.e., dystroglycans, syntrophins, and dystrobrevins [8,37]. However, to date, no dystrophin-DAP complex including an SGC has ever been found in the brain, although the expression patterns of the Dp427, Dp140, and Dp71 are totally overlapped with those of ε-SGs except for the neurons in the substantia nigra (Figs. 6 and 7). Besides ε-SGs, faint expression of β-, γ-, and δ-SG were found in whole brain materials at the transcriptional level [4,31,39,41]. We preliminarily tried to detect the SGs in the brain subcellular fractions containing ε-SGs by immunoblot, but found no evidence of their expression at the protein level (data not shown). In the central nervous system, especially in dorpaminergic neurons, the ε-SGs do not seem to form SGCs as a subcomplex of the dystrophin-DAP complex, but it is possible that the brain ε-SGs associate with other kinds of membrane proteins and/or cytoskeletal proteins in neuronal cells.

M-D is a movement disorder clinically characterized by myoclonus combined with dystonia. These abnormal movements can be caused by the pharmacological interference in dopaminergic and serotonergic neurotransmission. Indeed, dopa-responsive dystonia is caused by mutation in genes encoding enzymes of dopamine biosynthesis [19,24], and the transcript for *DYT1*, a gene responsible for early-onset torsion dystonia, is shown to be highly enriched in dopaminergic neurons in the substantia nigra [2]. Furthermore, a

point mutation in the gene for the dopamine D2 receptor was found in a family with M-D [23]. We demonstrated ε-SG expression in the dopaminergic neurons of the substantia nigra in mouse brain (Fig. 7). Biochemical fractionation of the brain homogenates suggested that some population of ε-SGs was present in synaptic membranes. These results raise the possibility that ε-SGs might be involved in the neuronal functions through dopaminergic transmission. However, besides the dopaminergic neurons, we detected ε-SG expression in neuronal cells in various brain regions (Figs. 6 and 7). Further studies for the expression of ε-SG among other types of neurons are necessary to elucidate the precise role of ε-SG in the central nervous system. A more recent study reported an M-D family with a novel mutation in the *SGCE* gene associated with epilepsy and/or electroencephalogram (EEG) abnormalities [15]. Interestingly, we found marked expression of ε-SGs in the cerebral cortex, hippocampus, and cerebellar cortex (Figs. 6 and 7), the location of lesions for some types of epilepsy [6,10,28]. It is therefore of interest to study the ε-SG expression in experimental models of epilepsy.

Disruption of the SGC including ε-SG1 does not produce obvious abnormalities in the peripheral nervous system [20], while it does induce vascular smooth muscle irregularities, which eventually cause cardiomyopathy [7]. Biochemical analysis for SGC formation [20] suggests that the loss-of-function mutations in the *SGCE* gene, reported in almost all M-D patients, would disrupt SGCs in the smooth muscle and Schwann cells. However, heart failure has not been reported in M-D patients, suggesting that differences exist between the pathophysiological mechanisms in the brain and smooth muscle in sarcoglycan deficiency.

In summary, we cloned and subsequently characterized two ε-SG isoforms, designated ε-SG1 and ε-SG2, in the brain. Our results strongly suggest that these isoforms play key functional roles in synaptic membranes of neuronal cells. Further investigation into the individual role of ε-SG isoforms would contribute to the understanding of the molecular mechanisms of M-D.

Acknowledgements

We thank Dr. Chihiro Akazawa for technical help for mouse brain dissection. This study was supported by a Health Science Research Grant, Research on 'Psychiatric and Neurological Diseases and Mental Health' (H12-kokoro-025), from the Ministry of Health, Labor and Welfare of Japan.

References

[1] K. Araishi, T. Sasaoka, M. Imamura, S. Noguchi, H. Hama, E. Wakabayashi, M. Yoshida, T. Hori, E. Ozawa, Loss of the sarcoglycan complex and sarcospan leads to muscular dystrophy in β-sarcoglycan-deficient mice, Hum. Mol. Genet. 8 (1999) 1589–1598.

[2] S.J. Augood, J.B. Penney Jr., I.K. Friberg, X.O. Breakefield, A.B. Young, L.J. Ozelius, D.G. Standaert, Expression of the early-onset torsion dystonia gene (DYT1) in human brain, Ann. Neurol. 43 (1998) 669–673.

[3] D.J. Blake, R. Nawrotzki, M.F. Peters, S.C. Froehner, K.E. Davies, Isoform diversity of dystrobrevin, the murine 87-kDa postsynaptic protein, J. Biol. Chem. 271 (1996) 7802–7810.

[4] C.G. Bönnemann, R. Modi, S. Noguchi, Y. Mizuno, M. Yoshida, E. Gussoni, E.M. McNally, D.J. Duggan, C. Angelini, E.P. Hoffman, E. Ozawa, L.M. Kunkel, β-Sarcoglycan (A3b) mutations cause autosomal recessive muscular dystrophy with loss of the sarcoglycan complex, Nat. Genet. 11 (1995) 266–273.

[5] T.J. Byers, H.G. Lidov, L.M. Kunkel, An alternative dystrophin transcript specific to peripheral nerve, Nat. Genet. 4 (1993) 77–81.

[6] I. Cohen, V. Navarro, S. Clemenceau, M. Baulac, R. Miles, On the origin of interictal activity in human temporal lobe epilepsy in vitro, Science 298 (2002) 1418–1421.

[7] R. Coral-Vazquez, R.D. Cohn, S.A. Moore, J.A. Hill, R.M. Weiss, R.L. Davisson, V. Straub, R. Barresi, D. Bansal, R.F. Hrstka, R. Williamson, K.P. Campbell, Disruption of the sarcoglycan–sarcospan complex in vascular smooth muscle: a novel mechanism for cardiomyopathy and muscular dystrophy, Cell 98 (1999) 465–474.

[8] K. Culligan, K. Ohlendieck, Diversity of the brain dystrophin–glycoprotein complex, J. Biomed. Biotechnol. 2 (2002) 31–36.

[9] L. Da Silva-Azevedo, O. Baum, A. Zakrzewicz, A.R. Pries, Vascular endothelial growth factor is expressed in endothelial cells isolated from skeletal muscles of nitric oxide synthase knockout mice during prazosin-induced angiogenesis, Biochem. Biophys. Res. Commun. 297 (2002) 1270–1276.

[10] R. Di Giaimo, M. Riccio, S. Santi, C. Galeotti, D.C. Ambrosetti, M. Melli, New insights into the molecular basis of progressive myoclonus epilepsy: a multiprotein complex with cystatin B, Hum. Mol. Genet. 11 (2002) 2941–2950.

[11] V.N. D'Souza, T.M. Nguyen, G.E. Morris, W. Karges, D.A. Pillers, P.N. Ray, A novel dystrophin isoform is required for normal retinal electrophysiology, Hum. Mol. Genet. 4 (1995) 837–842.

[12] A.W. Dunah, D.G. Standaert, Dopamine D1 receptor-dependent trafficking of striatal NMDA glutamate receptors to the postsynaptic membrane, J. Neurosci. 21 (2001) 5546–5558.

[13] J.M. Ervasti, K. Ohlendieck, S.D. Kahl, M.G. Gaver, K.P. Campbell, Deficiency of a glycoprotein component of the dystrophin complex in dystrophic muscle, Nature 345 (1990) 315–319.

[14] A.J. Ettinger, G. Feng, J.R. Sanes, ε-Sarcoglycan, a broadly expressed homologue of the gene mutated in limb-girdle muscular dystrophy 2D, J. Biol. Chem. 272 (1997) 32534–32538.

[15] E.M.J. Foncke, C. Klein, J.H.T.M. Koelman, P.L. Kramer, K. Schilling, B. Müller, J. Garrels, P. de Carvalho Aguiar, L. Liu, A. de Froe, J.D. Speelman, L.J. Ozelius, M.A.J. Tijssen, Hereditary myoclonus-dystonia associated with epilepsy, Neurology 60 (2003) 1988–1990.

[16] K.H. Holt, L.E. Lim, V. Straub, D.P. Venzke, F. Duclos, R.D. Anderson, B.L. Davidson, K.P. Campbell, Functional rescue of the sarcoglycan complex in the BIO 14.6 hamster using δ-sarcoglycan gene transfer, Mol. Cell 1 (1998) 841–848.

[17] J.P. Hugnot, H. Gilgenkrantz, N. Vincent, P. Chafey, G.E. Morris, A.P. Monaco, Y. Berwald-Netter, A. Koulakoff, J.C. Kaplan, A. Kahn, J. Chelly, Distal transcript of the dystrophin gene initiated from an alternative first exon and encoding a 75-kDa protein widely distributed in nonmuscle tissues, Proc. Natl. Acad. Sci. U. S. A. 89 (1992) 7506–7510.

[18] W.B. Huttner, W. Schiebler, P. Greengard, P. De Camilli, Synapsin I (protein I), a nerve terminal-specific phosphoprotein. III. Its association with synaptic vesicles studied in a highly purified synaptic vesicle preparation, J. Cell Biol. 96 (1983) 1374–1388.

[19] H. Ichinose, T. Ohye, E. Takahashi, N. Seki, T. Hori, M. Segawa, Y. Nomura, K. Endo, H. Tanaka, S. Tsuji, K. Fujita, T. Nagatsu, Hereditary progressive dystonia with marked diurnal fluctuation caused

by mutations in the GTP cyclohydrolase I gene, Nat. Genet. 8 (1994) 236–242.
[20] M. Imamura, K. Araishi, S. Noguchi, E. Ozawa, A sarcoglycan-dystroglycan complex anchors Dp116 and utrophin in the peripheral nervous system, Hum. Mol. Genet. 9 (2000) 3091–3100.
[21] Y. Iwata, H. Nakamura, Y. Mizuno, M. Yoshida, E. Ozawa, M. Shigekawa, Defective association of dystrophin with sarcolemmal glycoproteins in the cardiomyopathic hamster heart, FEBS Lett. 329 (1993) 227–231.
[22] P.J. Kahle, M. Neumann, L. Ozmen, V. Muller, H. Jacobsen, A. Schindzielorz, M. Okochi, U. Leimer, H. van Der Putten, A. Probst, E. Kremmer, H.A. Kretzschmar, C. Haass, Subcellular localization of wild-type and Parkinson's disease-associated mutant α-synuclein in human and transgenic mouse brain, J. Neurosci. 20 (2000) 6365–6373.
[23] C. Klein, M.F. Brin, P. Kramer, M. Sena-Esteves, D. de Leon, D. Doheny, S. Bressman, S. Fahn, X.O. Breakefield, L.J. Ozelius, Association of a missense change in the D2 dopamine receptor with myoclonus dystonia, Proc. Natl. Acad. Sci. U. S. A. 96 (1999) 5173–5176.
[24] P.M. Knappskog, T. Flatmark, J. Mallet, B. Lüdecke, K. Bartholome, Recessively inherited L-DOPA-responsive dystonia caused by a point mutation (Q381K) in the tyrosine hydroxylase gene, Hum. Mol. Genet. 4 (1995) 1209–1212.
[25] J. Kyhse-Andersen, Electroblotting of multiple gels: a simple apparatus without buffer tank for rapid transfer of proteins from polyacrylamide to nitrocellulose, J. Biochem. Biophys. Methods 10 (1984) 203–209.
[26] U.K. Laemmli, Cleavage of structural proteins during the assembly of the head of bacteriophage T4, Nature 227 (1970) 680–685.
[27] D. Lederfein, Z. Levy, N. Augier, D. Mornet, G. Morris, O. Fuchs, D. Yaffe, U. Nudel, A 71-kilodalton protein is a major product of the Duchenne muscular dystrophy gene in brain and other nonmuscle tissues, Proc. Natl. Acad. Sci. U. S. A. 89 (1992) 5346–5350.
[28] C. Leroy, C. Roch, E. Koning, I.J. Namer, A. Nehlig, In the lithium-pilocarpine model of epilepsy, brain lesions are not linked to changes in blood–brain barrier permeability: an autoradiographic study in adult and developing rats, Exp. Neurol. 182 (2003) 361–372.
[29] H.G.W. Lidov, T.J. Byers, S.C. Watkins, L.M. Kunkel, Localization of dystrophin to postsynaptic regions of central nervous system cortical neurons, Nature 348 (1990) 725–728.
[30] H.G.W. Lidov, S. Selig, L.M. Kunkel, Dp140: a novel 140 kDa CNS transcript from the dystrophin locus, Hum. Mol. Genet. 4 (1995) 329–335.
[31] L.E. Lim, F. Duclos, O. Broux, N. Bourg, Y. Sunada, V. Allamand, J. Meyer, I. Richard, C. Moomaw, C. Slaughter, F.M.S. Tomé, M. Fardeau, C.E. Jackson, J.S. Beckman, K.P. Campbell, β-Sarcoglycan: characterization and role in limb-girdle muscular dystrophy linked to 4q12, Nat. Genet. 11 (1995) 257–265.
[32] L.A. Liu, E. Engvall, Sarcoglycan isoform in skeletal muscle, J. Biol. Chem. 274 (1999) 38171–38176.
[33] E.M. McNally, C.T. Ly, L.M. Kunkel, Human ε-sarcoglycan is highly related to α-sarcoglycan (adhalin), the limb girdle muscular dystrophy 2D gene, FEBS Lett. 422 (1998) 27–32.
[34] M.F. Mehler, Brain dystrophin, neurogenetics and mental retardation, Brain Res. Rev. 32 (2000) 277–307.
[35] Y. Mizuno, M. Yoshida, H. Yamamoto, S. Hirai, E. Ozawa, Distribution of dystrophin isoforms and dystrophin-associated proteins 43DAG (A3a) and 50DAG (A2) in various monkey tissues, J. Biochem. (Tokyo) 114 (1993) 936–941.
[36] Y. Mizuno, S. Noguchi, H. Yamamoto, M. Yoshida, A. Suzuki, Y. Hagiwara, Y.K. Hayashi, K. Arahata, I. Nonaka, S. Hirai, E. Ozawa, Selective defect of sarcoglycan complex in severe childhood autosomal recessive muscular dystrophy muscle, Biochem. Biophys. Res. Commun. 203 (1994) 979–983.
[37] H. Moukhles, S. Carbonetto, Dystroglycan contributes to the formation of multiple dystrophin-like complexes in brain, J. Neurochem. 78 (2001) 824–834.
[38] V. Nigro, E.S. Moreira, G. Piluso, M. Vainzof, A. Belsito, L. Politano, A.A. Puca, M.R. Passos-Bueno, M. Zatz, Autosomal recessive limb-girdle muscular dystrophy, LGMD2F, is caused by a mutation in the δ-sarcoglycan gene, Nat. Genet. 14 (1996) 195–198.
[39] V. Nigro, Y. Okazaki, A. Belsito, G. Piluso, Y. Matsuda, L. Politano, G. Nigro, C. Ventura, C. Abbondanza, A.M. Molinari, D. Acampora, M. Nishimura, Y. Hayashizaki, G.A. Puca, Identification of the Syrian hamster cardiomyopathy gene, Hum. Mol. Genet. 6 (1997) 601–607.
[40] S. Noguchi, E.M. McNally, K. Ben Othmane, Y. Hagiwara, Y. Mizuno, M. Yoshida, H. Yamamoto, C.G. Bönnemann, E. Gussoni, P.H. Denton, T. Kyriakides, L. Middleton, F. Hentati, M. Ben Hamida, I. Nonaka, J.M. Vance, L.M. Kunkel, E. Ozawa, Mutations in the dystrophin-associated protein γ-sarcoglycan in chromosome 13 muscular dystrophy, Science 270 (1995) 819–822.
[41] S. Noguchi, E. Wakabayashi-Takai, T. Sasaoka, E. Ozawa, Analysis of the spatial, temporal and tissue-specific transcription of γ-sarcoglycan gene using a transgenic mouse, FEBS Lett. 495 (2001) 77–81.
[42] E. Ozawa, S. Noguchi, Y. Mizuno, Y. Hagiwara, M. Yoshida, From dystrophinopathy to sarcoglycanopathy: evolution of a concept of muscular dystrophy, Muscle Nerve 21 (1998) 421–438.
[43] E. Ozawa, M. Imamura, S. Noguchi, M. Yoshida, Dystrophinopathy and sarcoglycanopathy, Neurosci. News 3 (2000) 13–19.
[44] G.R. Phillips, J.K. Huang, Y. Wang, H. Tanaka, L. Shapiro, W. Zhang, W.S. Shan, K. Arndt, M. Frank, R.E. Gordon, M.A. Gawinowicz, Y. Zhao, D.R. Colman, The presynaptic particle web: ultrastructure composition, dissolution, and reconstitution, Neuron 32 (2001) 63–77.
[45] S.L. Roberds, F. Leturcq, V. Allamand, F. Piccolo, M. Jeanpierre, R.D. Anderson, L.E. Lim, J.C. Lee, F.M. Tomé, N.B. Romero, M. Fardeau, J.S. Beckmann, J.-C. Kaplan, K.P. Campbell, Missense mutations in the adhalin gene linked to autosomal recessive muscular dystrophy, Cell 78 (1994) 625–633.
[46] R. Saunders-Pullman, J. Shriberg, G. Heiman, D. Raymond, K. Wendt, P. Kramer, K. Schilling, R. Kurlan, C. Klein, L.J. Ozelius, N.J. Risch, S.B. Bressman, Myoclonus dystonia: possible association with obsessive-compulsive disorder and alcohol dependence, Neurology 58 (2002) 242–245.
[47] V. Straub, A.J. Ettinger, M. Durbeej, D.P. Venzke, S. Cutshall, J.R. Sanes, K.P. Campbell, ε-Sarcoglycan replaces α-sarcoglycan in smooth muscle to form a unique dystrophin-glycoprotein complex, J. Biol. Chem. 274 (1999) 27989–27996.
[48] M. Yoshida, E. Ozawa, Glycoprotein complex anchoring dystrophin to sarcolemma, J. Biochem. (Tokyo) 108 (1990) 748–752.
[49] M. Yoshida, A. Suzuki, H. Yamamoto, S. Noguchi, Y. Mizuno, E. Ozawa, Dissociation of the complex of dystrophin and its associated proteins into several unique groups by n-octyl β-D-glucoside, Eur. J. Biochem. 222 (1994) 1055–1061.
[50] M. Yoshida, H. Hama, M. Ishikawa-Sakurai, M. Imamura, Y. Mizuno, K. Araishi, E. Wakabayashi-Takai, S. Noguchi, T. Sasaoka, E. Ozawa, Biochemical evidence for association of dystrobrevin with the sarcoglycan-sarcospan complex as a basis for understanding sarcoglycanopathy, Hum. Mol. Genet. 9 (2000) 1033–1040.
[51] A. Zimprich, M. Grabowski, F. Asmus, M. Naumann, D. Berg, M. Bertram, K. Scheidtmann, P. Kern, J. Winkelmann, B. Muller-Myhsok, L. Riedel, M. Bauer, T. Muller, M. Castro, T. Meitinger, T.M. Strom, T. Gasser, Mutations in the gene encoding ε-sarcoglycan cause myoclonus-dystonia syndrome, Nat. Genet. 29 (2001) 66–69.

THE JOURNAL OF BIOLOGICAL CHEMISTRY
Vol. 279, No. 15, Issue of April 9, pp. 15091–15095, 2004
Printed in U.S.A.

α1-Syntrophin Modulates Turnover of ABCA1*

Received for publication, December 9, 2003, and in revised form, January 8, 2004
Published, JBC Papers in Press, January 13, 2004, DOI 10.1074/jbc.M313436200

Youichi Munehira‡§, Tomohiro Ohnishi‡§, Shinobu Kawamoto¶, Akiko Furuya¶, Kenya Shitara¶, Michihiro Imamura‖, Toshifumi Yokota‖, Shin'ichi Takeda‖, Teruo Amachi‡, Michinori Matsuo‡, Noriyuki Kioka‡, and Kazumitsu Ueda‡

From the ‡Laboratory of Cellular Biochemistry, Division of Applied Life Sciences, Graduate School of Agriculture, Kyoto University, Kyoto 606-8502, Japan, the ¶Tokyo Research Laboratories, Kyowa Hakko Kogyo Company Limited, Machida, Tokyo 194-8533, Japan, and the ‖National Institute of Neuroscience, National Center of Neurology and Psychiatry, 4-1-1 Ogawa-higashi, Kodaira, Tokyo 187-8502, Japan

ABCA1 (ATP-binding cassette transporter A1) mediates the release of cellular cholesterol and phospholipid to form high density lipoprotein. Functions of ABCA1 are highly regulated at the transcriptional and post-transcriptional levels, and the synthesized ABCA1 protein turns over rapidly with a half-life of 1–2 h. To examine whether the functions of ABCA1 are modulated by associated proteins, a yeast two-hybrid library was screened with the C-terminal 120 amino acids of ABCA1. Two PDZ (PSD95-Discs large-ZO1) proteins, α1-syntrophin and Lin7, were found to interact with ABCA1. Immunoprecipitation revealed that α1-syntrophin interacted with ABCA1 strongly and that the interaction was via the C-terminal three amino acids SYV of ABCA1. Co-expression of α1-syntrophin in human embryonic kidney 293 cells retarded degradation of ABCA1 and made the half-life of ABCA1 five times longer than in the cells not expressing α1-syntrophin. This effect is not common among PDZ-containing proteins interacting with ABCA1, because Lin7, which was also found to interact with the C terminus region of ABCA1, did not have a significant effect on the half-life of ABCA1. Co-expression of α1-syntrophin significantly increased the apoA-I-mediated release of cholesterol. ABCA1 was co-immunoprecipitated with α1-syntrophin from mouse brain. These results suggest that α1-syntrophin is involved in intracellular signaling, which determines the stability of ABCA1 and modulates cellular cholesterol release.

Cholesterol is not catabolized in the peripheral cells and, therefore, is mostly released and transported to the liver for conversion to bile acids to maintain cholesterol homeostasis. The same pathway may also remove cholesterol that has pathologically accumulated in cells, such as at the initial stage of atherosclerosis. The assembly of high density lipoprotein (HDL)[1] particles by lipid-free apolipoproteins with cellular lipid has been recognized as one of the major mechanisms for the cellular cholesterol release (1, 2). ApoA-I-mediated cholesterol efflux is a major event in "reverse cholesterol transport," a process that generates HDL and transports excess cholesterol from the peripheral tissues, including the arterial wall, to the liver for biliary secretion. The importance of ABCA1 in this active cholesterol-releasing pathway for regulating cholesterol homeostasis became apparent with the finding that it is impaired in the cells from patients with Tangier disease, a genetic deficiency of circulating HDL (3, 4). Tangier disease is caused by mutations in ABCA1. ABCA1 mutations are also a cause of familial HDL deficiency and are associated with premature atherosclerosis (5, 6).

Cholesterol is a prerequisite for cells, but, at the same time, the hyper-accumulation of cholesterol is harmful to cells. Therefore, the expression of ABCA1 is highly regulated at both the transcriptional and post-transcriptional level. The transcription of ABCA1 is regulated by the intracellular oxysterol concentration via the LXR/RXR nuclear receptor (7), and the synthesized ABCA1 protein turns over rapidly with a half-life of 1–2 h (8–10). However, the post-translation regulatory mechanism of ABCA1 is unclear. We analyzed the associated proteins that could be involved in the post-translational regulation of ABCA1. By yeast two-hybrid screening with the C-terminal 120 amino acids of ABCA1, two PDZ (PSD95-Discs large-ZO1)-binding proteins, α1-syntrophin and Lin7, were found to interact with ABCA1. Immunoprecipitation confirmed the association of α1-syntrophin and ABCA1 via its C-terminal amino acids. The importance of this interaction in the regulation of ABCA1 function was examined.

EXPERIMENTAL PROCEDURES

Materials—The anti-ABCA1 monoclonal antibody KM3073 was generated against the first extracellular domain of the human ABCA1 protein in rats. Anti-ABCA1 monoclonal antibody KM3110 was generated against the C-terminal 20 amino acids of ABCA1 in mice. Anti-ABCA1 polyclonal antibody, previously described (11), was used for immunostaining. Affinity-purified antibody specific for α1-syntrophin was prepared using recombinant proteins. Human α1-syntrophin (amino acids 169–346) was fused to glutathione *S*-transferase (GST) in the pGEX vector (Amersham Biosciences) and to the maltose-binding protein (MBP) in the pMAL-c2 vector (New England Biolabs, Inc.). The GST-α1-syntrophin protein was used as an antigen. Obtained rabbit antiserum was affinity purified with the column coupled with the MBP-α1-syntrophin fusion protein. Anti-FLAG epitope monoclonal antibody M2 was purchased from Sigma. Human apoA-I was a gift from Dr. Shinji Yokoyama, Nagoya City University Graduate School of Medical Sciences.

Animals—16-week-old α1-syntrophin (−/−) (12) and wild-type C57BL/6 mice were used in this study. The animals were allowed *ad libitum* access to food and drinking water. Mice carrying mutations were identified by Southern blot analysis as described (12).

Yeast Two-hybrid Library Screening—The Matchmaker Two-hybrid

* This work was supported by Grant-in-aid for Creative Scientific Research 15GS0301 from the Ministry of Education, Culture, Sports, Science, and Technology of Japan, the Bio-oriented Technology Research Advancement Institution (BRAIN), and the Nakajima Foundation. The costs of publication of this article were defrayed in part by the payment of page charges. This article must therefore be hereby marked "*advertisement*" in accordance with 18 U.S.C. Section 1734 solely to indicate this fact.

§ These authors contributed equally to this work.

** To whom correspondence should be addressed. Tel.: 81-75-753-6105; Fax: 81-75-753-6104; E-mail: uedak@kais.kyoto-u.ac.jp.

[1] The abbreviations used are: HDL, high density lipoprotein; ABCA1, ATP-binding cassette transporter A1; HEK293, human embryonic kidney 293; LXR/RXR, liver X receptor/retinoid X receptor; PBS, phosphate-buffered saline; PDZ, PSD95-Discs large-ZO1.

System 3 from Clontech was used following the manufacturer's instructions. The ABCA1 C terminus region coding for 120 amino acids was cloned from cDNA (13) in pGBKT7. The yeast strain AH109, transformed with pGBKT7/ABCA1-C120, was mated with the yeast strain Y187, which had been pretransformed with a human bone marrow cDNA library. The plasmids, purified from β-galactosidase positive clones, were transformed into *Escherichia coli* and sequenced.

Cellular Lipid Release Assay—Cells were subcultured in poly-L-Lys-coated 6-well plates at a density of 1.0×10^6 cells in Dulbecco's modified Eagle's medium supplemented with 10% (v/v) fetal bovine serum. After 24 h, cells were transfected with ABCA1 and/or FLAG-α1-syntrophin using LipofectAMINE (Invitrogen). After 24 h of incubation, the cells were washed with phosphate-buffered saline (PBS) and incubated in 0.02% bovine serum albumin in Dulbecco's modified Eagle's medium with 10 μg/ml apoA-I. The lipid content in the medium was determined after 24 h incubation as described previously (14).

Immunoprecipitation Analysis—HEK293 cells, transiently expressing ABCA1, were lysed with PBS containing 1% Triton X-100 and protease inhibitors (100 μg/ml 4-(amidino)-phenylmethanesulfonyl fluoride hydrochloride (pAPMSF)), 10 μg/ml leupeptin, and 2 μg/ml aprotinin). Equal amounts of total protein were incubated with 5 μg of anti-FLAG antibody M2 for 1 h at 4 °C. Brain of normal mice and mice lacking α1-syntrophin (α1-*Syn*$^{-/-}$) (12) was homogenized in ice-cold homogenization buffer (10 mM sodium phosphate, 0.4 M NaCl, 5 mM EDTA, pH 7.8, and the protease inhibitors). The particulate fraction was pelleted by centrifugation (12,000 × *g* for 10 min), resuspended in 10 volumes of homogenization buffer, and recentrifuged. Washed pellets were solubilized in homogenization buffer containing 1% Triton X-100 and incubated on ice for 30 min. The suspension was centrifuged again, and the supernatant was then incubated with anti-α1-syntrophin rabbit polyclonal antibody for 100 min at 4 °C. The immunocomplexes were incubated with protein G-Sepharose (Sigma) for 1 h and washed four times with homogenization buffer containing 1% Triton X-100. The bound proteins were separated by SDS-PAGE (7%) and analyzed by immunoblotting using the anti-ABCA1 antibody KM3073 or KM3110.

Immunostaining—HEK293 cells were co-transfected with ABCA1 and FLAG-tagged α1-syntrophin or FLAG-tagged Lin7 using LipofectAMINE. The cells were fixed in 4% paraformaldehyde and 5% sucrose in PBS$^+$ (PBS with 0.87 mM $CaCl_2$ and 0.49 mM $MgCl_2$) for 30 min and permeabilized for 5 min in 0.4% Triton X-100 in PBS$^+$. The cells were blocked with 10% goat serum diluted with PBS$^+$. This was followed by incubation with anti-ABCA1 polyclonal antibody and anti-FLAG M2 antibody. The cells were then stained with Alexa 488-labeled anti-rat IgG antibody and Alexa 564-labeled anti-mouse IgG antibody (Molecular Probes) as secondary antibodies. The fluorescence images were obtained using an Axiovert microscope (Carl Zeiss) equipped with a MicroRadiance confocal laser-scanning microscope (Bio-Rad).

RESULTS

ABCA1 Interacts with Two PDZ-binding Proteins—To search for proteins that are associated with the C-terminal region of ABCA1, a fusion construct of the Gal4 DNA-binding domain with the C-terminal 120 amino acids of human ABCA1 was used as bait for two-hybrid screening. The identified genes contained two PDZ-containing proteins, α1-syntrophin (10 clones) and Lin7 (two clones). To determine whether the interaction between ABCA1 and α1-syntrophin or Lin7 occurs *in vivo*, we transfected FLAG-tagged α1-syntrophin, FLAG-tagged Lin7, or FLAG-tagged vinexin β (15) (as a negative control) together with ABCA1 into HEK293 cells. Lysates prepared from transfected cells were immunoprecipitated with anti-FLAG antibody, and precipitates were evaluated by immunoblotting with anti-ABCA1 antibody. As shown in Fig. 1, ABCA1 was co-immunoprecipitated with FLAG-tagged α1-syntrophin or FLAG-tagged Lin7, but not with FLAG-tagged vinexin β. ABCA1 was not precipitated with mouse IgG control from any of the lysates in which the expression of ABCA1 (Fig. 1) and FLAG-tagged proteins (data not shown) were detected by immunoblotting. More than 25% of the ABCA1 expressed in HEK293 was roughly estimated to be co-immunoprecipitated with FLAG-tagged α1-syntrophin, suggesting strong interaction between ABCA1 and α1-syntrophin (Fig. 2). The interaction between ABCA1 and Lin7 seemed to be weak, because the amount of precipitated ABCA1 with Lin7 was much less than that with α1-syntrophin. The amount of ABCA1 in lysates was consistently higher when co-expressed with α1-syntrophin than with other proteins.

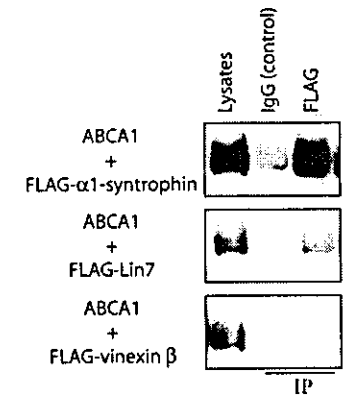

FIG. 1. ***In vivo* association of ABCA1 with α1-syntrophin.** HEK293 cells were co-transfected with human ABCA1 and FLAG-tagged α1-syntrophin, FLAG-tagged Lin7, or FLAG-tagged vinexin β. Cell lysates were immunoprecipitated (*IP*) with anti-FLAG antibody. Immunocomplexes and cell lysates (5%) were subjected to immunoblotting using Anti-ABCA1 monoclonal antibody KM3110, generated against the C-terminal 20 amino acids of ABCA1. Mouse IgG was used as a negative control. The data are representative of three independent experiments.

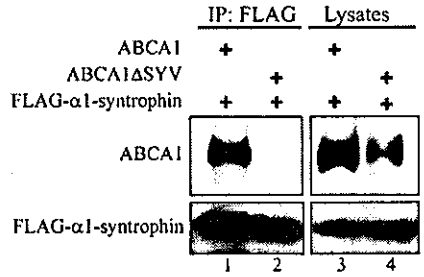

FIG. 2. **ABCA1 interacts with α1-syntrophin via the C-terminal three amino acids.** HEK293 cells were co-transfected with ABCA1 or ABCA1ΔSYV, in which the C-terminal three amino acids were trimmed, and with FLAG-tagged α1-syntrophin. Cell lysates were immunoprecipitated (*IP*) with anti-FLAG antibody. Immunocomplexes and cell lysates (5%) were subjected to immunoblotting using the anti-ABCA1 monoclonal antibody KM3073, generated against the first extracellular domain of the human ABCA1, and an anti-FLAG antibody. The data are representative of two independent experiments.

ABCA1 Interacts with α1-Syntrophin via the C-terminal Three Amino Acids—ABCA1 contains the amino acid sequence ESYV at the C terminus, which has been described as a binding target for syntrophin PDZ domains (16). To determine whether the C-terminal three amino acids SYV are important for the interaction, ABCA1ΔSYV, in which these amino acids were trimmed, was co-expressed with FLAG-tagged α1-syntrophin in HEK293 cells. Although the expression of ABCA1ΔSYV was detected in the lysates, no ABCA1ΔSYV was co-precipitated with FLAG-tagged α1-syntrophin. These results suggest that the interaction is mediated with the C-terminal three amino acids SYV of ABCA1 and α1-syntrophin PDZ domains.

Co-localization of the ABCA1 and PDZ-containing Proteins α1-Syntrophin and Lin7—ABCA1 is mainly localized to plasma membrane but is also substantially expressed in intracellular compartments (11, 17–20). To determine whether ABCA1 and α1-syntrophin or Lin7 are co-localized in cells, ABCA1 was co-transfected with FLAG-tagged α1-syntrophin or FLAG-tagged Lin7 into HEK293 cells. The subcellular localization of these proteins was examined under a confocal laser scanning microscope. α1-Syntrophin resided mainly on plasma mem-

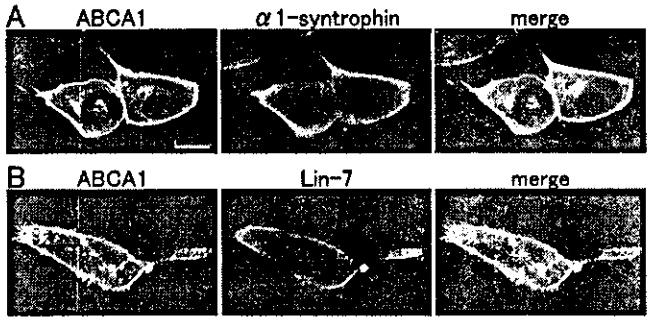

FIG. 3. **Co-localization of ABCA1 and PDZ-containing proteins, α1-syntrophin and Lin7.** HEK293 cells were co-transfected with ABCA1 and FLAG-tagged α1-syntrophin or FLAG-tagged Lin7. The cells were fixed in 4% paraformaldehyde and 5% sucrose, permeabilized in 0.4% Triton X-100, and then doubly stained with anti-ABCA1 polyclonal antibody (*left*) and anti-FLAG antibody (*middle*). A merged image of the staining (*green*, ABCA1; *red*, α1-syntrophin) is also shown (*right*). The data are representative of three independent experiments. *Bar*, 10 μm

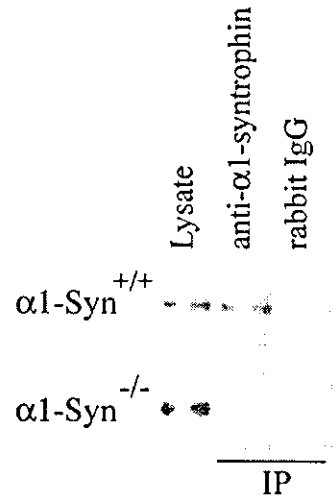

FIG. 4. **Physiological association of mouse ABCA1 with α1-syntrophin.** Brain lysates prepared from normal mouse or α1-syntrophin (−/−) were immunoprecipitated (*IP*) with anti-α1-syntrophin antibody. Immunocomplexes and cell lysates (1%) were subjected to immunoblotting using anti-ABCA1 antibody KM3110. Rabbit IgG was used as a negative control. The data are representative of three independent experiments.

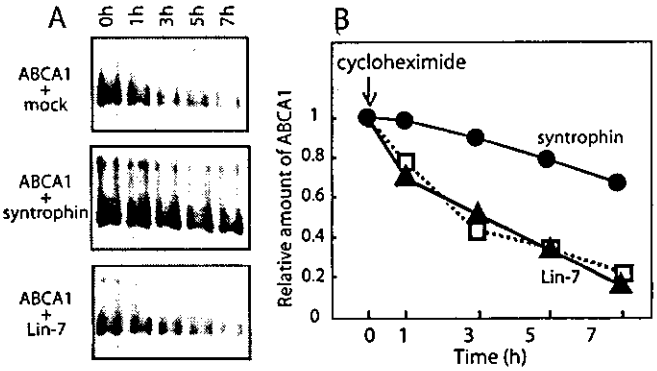

FIG. 5. **α1-Syntrophin modulates turnover of ABCA1.** *A*, HEK293 cells were co-transfected with ABCA1 and vector (*mock*), FLAG-tagged α1-syntrophin, or FLAG-tagged Lin7. At 48 h after transfection, 100 μg/ml of cycloheximide was added to block protein synthesis. After the indicated times, cell lysates were subjected to immunoblotting using Anti-ABCA1 monoclonal antibody KM3110. *B*, quantitation of ABCA1 levels. Values are expressed as fold increase with respect to the amount of ABCA1 just before adding cycloheximide. □, mock transfected; ●, co-transfected with α1-syntrophin; ▲, co-transfected with Lin7. The data are representative of two experiments with similar results.

brane, where it co-localized with ABCA1 (Fig. 3*A*). Lin7 also localized mainly on plasma membrane and appeared not to be uniformly distributed but rather clustered in a specific region of plasma membrane in some cells. In those regions, high expression of ABCA1 and the formation of filopodia were observed (Fig. 3*B*).

Interaction of α1-Syntrophin with ABCA1 in Mouse Brain—Among syntrophin isoforms, α1-syntrophin is mainly expressed in brain, skeletal muscle, and heart in mouse (21). To examine whether ABCA1 and α1-syntrophin interact physiologically, we tried co-immunoprecipitation of these two proteins from mouse brain. Lysates prepared from mouse brain were immunoprecipitated with anti-α1-syntrophin antibody, and precipitates were evaluated by immunoblotting with anti-ABCA1 antibody. As shown in Fig. 4, mouse ABCA1 was co-immunoprecipitated with α1-syntrophin, but not with control IgG. This interaction was confirmed to be specific, because ABCA1 was not precipitated from brain of α1-*Syn*$^{-/-}$ mice (Fig. 4).

α1-Syntrophin Modulates Turnover of ABCA1—Syntrophins have been reported to be involved in protein stability. For example, interaction with β2-syntrophin controls the degradation of ICA512, which connects insulin secretory granules to the utrophin complex and the actin cytoskeleton, by calpain (22), and the stability of AQP4 (23) and neuronal nitric-oxide synthase (12) is suggested as being controlled by α1-syntrophin. The amount of ABCA1 in lysates was consistently higher on co-expression with α1-syntrophin than with other proteins as shown in Fig. 1. Therefore, we examined the effect of α1-syntrophin on the stability of ABCA1. FLAG-tagged α1-syntrophin or FLAG-tagged Lin7 was transiently co-expressed with ABCA1 in HEK293 cells. At 48 h after transfection, the medium was replaced with 10% fetal bovine serum/Dulbecco's modified Eagle's medium containing 100 μg/ml cycloheximide, and cellular protein synthesis was inhibited to block supply of the newly synthesized ABCA1. After the indicated times, the amount of ABCA1 was measured by immunoblotting (Fig. 5*A*). After the inhibition of cellular protein synthesis, 80% of ABCA1 was degraded in 7 h, and the half-life was about 2 h as reported previously (10). Thus, ABCA1 protein turns over rapidly in HEK293 cells. When ABCA1 was co-expressed with α1-syntrophin, only ~30% of ABCA1 was degraded in a 7-h treatment with cycloheximide, and the half-life was estimated to be 10 h (Fig. 5*B*). Lin7, which is a PDZ protein and also binds to the C terminus region of ABCA1, did not show a significant effect on the half-life of ABCA1. The half-life of ABCA1ΔSYV was scarcely affected by co-expression of α1-syntrophin (data not shown). These results suggest that α1-syntrophin decreases ABCA1 protein degradation by interacting with the C terminus three amino acids of ABCA1.

α1-Syntrophin Increases apoA-I-mediated Cholesterol Efflux by ABCA1—To analyze the functional consequences of decreased ABCA1 protein degradation in the presence of α1-syntrophin, the apoA-I-mediated release of cholesterol was examined from HEK293 cells transiently cotransfected with ABCA1 and α1-syntrophin (Fig. 6). Human ABCA1 transiently expressed in HEK293 cells supported the apoA-I-mediated release of cholesterol as previously reported with ABCA1-green fluorescent protein (13). Co-expression of α1-syntrophin significantly increased the apoA-I-mediated release of cholesterol, although expression of α1-syntrophin alone did not affect it.

DISCUSSION

In this study, we identified α1-syntrophin as a protein interacting strongly with ABCA1 via the C-terminal three amino

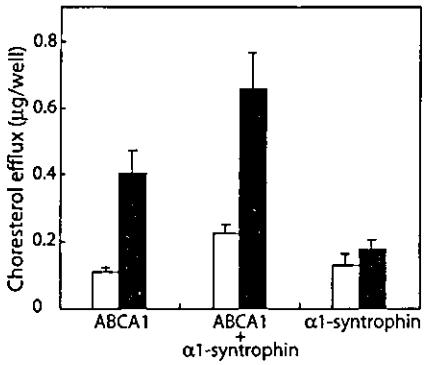

FIG. 6. **Effects of α1-syntrophin co-expression on apoA-I-mediated cholesterol transport.** The cholesterol content of the medium in 6-well plates containing HEK293 cells transiently transfected with ABCA1 alone, ABCA1 and α1-syntrophin, and α1-syntrophin alone was measured after 24 h incubation in the presence (*black bars*) or absence (*white bars*) of 10 μg/ml of apoA-I.

acids SYV of ABCA1. Co-expression of α1-syntrophin retarded degradation of ABCA1 and made the half-life of ABCA1 in HEK293 cells five times longer than in the cells not expressing α1-syntrophin. This effect is not common among PDZ-containing proteins interacting with ABCA1, because Lin7, which also binds to the C terminus region of ABCA1, did not show a similar effect. Co-expression of α1-syntrophin significantly increased the apoA-I-mediated release of cholesterol. Because this interaction was observed in mouse brain, α1-syntrophin could be involved in lipid homeostasis in brain.

Mammalian cells have developed sophisticated mechanisms to ensure adequate cellular cholesterol levels, because cholesterol plays a critical role in several important cell functions, including protein trafficking, membrane vesiculation, and signal transduction, and, at the same time, hyper-accumulation of cholesterol is harmful for cells. Plasma membrane cholesterol content, for example, is regulated through a feedback mechanism controlled by sterol regulatory element binding protein-2 (SREBP-2) (24, 25). To eliminate excess cholesterol from the cell, expression of ABCA1, a key molecule for apoA-I-mediated cholesterol efflux, is stimulated by intracellular oxysterol via the LXR/RXR nuclear receptor (26). The synthesized ABCA1 protein turns over rapidly with a half-life of 1–2 h (8, 10) to cancel cholesterol efflux by ABCA1. Because co-expression of α1-syntrophin retarded degradation of ABCA1 and made the half-life of ABCA1 in HEK293 cells five times longer than in the cells not expressing α1-syntrophin, α1-syntrophin is expected to be involved in intracellular signaling, which determines the stability of ABCA1.

Recently, it has been proposed that ABCA1 is regulated in two different ABCA1 degradation pathways under various cellular conditions: (i) a basal calpain degradation pathway that is turned off by interaction with apolipoproteins (9, 10); and (ii) a ubiquitin-proteasome pathway that is activated by marked free cholesterol loading (27). A sequence rich in proline, glutamate, serine, and threonine (PEST sequence) just before the second membrane spanning domain of ABCA1 (amino acid residue 1283–1306) is involved in regulating the calpain degradation of ABCA1 (10). Although the nature of the apoA-I-ABCA1 interaction is not fully understood, conformational alteration of ABCA1 through the PEST sequence may be induced by its direct or indirect interaction with apoA-I, which may render ABCA1 resistant to proteolysis by calpain. Because ABCA1 was ubiquitinated as well when co-expressed with α1-syntrophin (data not shown), α1-syntrophin seems not to affect ABCA1 degradation in an ubiquitin-proteasome pathway. Binding of α1-syntrophin to the C terminus of ABCA1 may cause a conformational alteration similar to that caused by apoA-I binding and render ABCA1 resistant to proteolysis by calpain.

Syntrophins are a family of five proteins (α1, β1, β2, γ1, and γ2,) containing two pleckstrin homology domains, a PDZ domain, and a C-terminal syntrophin-unique region (28). Analysis of α-*Syn*$^{-/-}$ mouse has demonstrated that perivascular localization of AQP4 in brain requires α1-syntrophin (23) and that the stability of AQP4 (23) and neuronal nitric-oxide synthase (12) decreases in the absence of α1-syntrophin. β2-syntrophin was also reported to interact with ABCA1 and was proposed to participate in the retaining of ABCA1 in cytoplasmic vesicles by forming a ABCA1-β2-syntrophin-utrophin complex (29). It is possible that α1-syntrophin is also involved in endocytotic recycling of ABCA1. Extracellular lipid-free apoA-I may first interact with ABCA1 on plasma membrane, but it is not clear whether the formation of HDL takes place extracellularly or if intracellular events, such as endocytotic recycling, are involved (30). It is intriguing that apoA-I and α1-syntrophin have a similar effect on ABCA1 turnover. A mutation of ABCA1 that causes Tangier disease (W590S) does not affect apoA-I binding or initial ATP binding/hydrolysis but results in a defect in lipid efflux (11, 31, 32). Because apoA-I failed to affect calpain degradation of ABCA1-W590S in HEK293 cells (10), additional signals following apoA-I binding to ABCA1 are speculated to be necessary for the subsequent inhibition of calpain degradation. It is possible that PDZ-containing proteins such as α1-syntrophin are involved in intracellular signaling, which determines the stability of ABCA1.

Acknowledgments—We thank Dr. Shinji Yokoyama for providing lipid-free apoA-I and for helpful discussion. We also thank Dr. Sumiko Abe-Dohmae for technical guidance.

REFERENCES

1. Hara, H., and Yokoyama, S. (1991) *J. Biol. Chem.* **266,** 3080–3086
2. Yokoyama, S. (2000) *Biochim. Biophys. Acta* **1529,** 231–244
3. Francis, G. A., Knopp, R. H., and Oram, J. F. (1995) *J. Clin. Investig.* **96,** 78–87
4. Remaley, A. T., Schumacher, U. K., Stonik, J. A., Farsi, B. D., Nazih, H., and Brewer, H. B., Jr. (1997) *Arterioscler. Thromb. Vasc. Biol.* **17,** 1813–1821
5. Brooks-Wilson, A., Marcil, M., Clee, S., Zhang, L., Roomp, K., van Dam, M., Yu, L., Brewer, C., Collins, J., Molhuizen, H., Loubser, O., Ouelette, B., Fichter, K., Ashbourne-Excoffon, K., Sensen, C., Scherer, S., Mott, S., Denis, M., Martindale, D., Frohlich, J., Morgan, K., Koop, B., Pimstone, S., Kastelein, J., and Hayden, M. (1999) *Nat. Genet.* **22,** 336–345
6. Attie, A. D., Kastelein, J. P., and Hayden, M. R. (2001) *J. Lipid Res.* **42,** 1717–1726
7. Venkateswaran, A., Laffitte, B. A., Joseph, S. B., Mak, P. A., Wilpitz, D. C., Edwards, P. A., and Tontonoz, P. (2000) *Proc. Natl. Acad. Sci. U. S. A.* **97,** 12097–12102
8. Wang, Y., and Oram, J. F. (2002) *J. Biol. Chem.* **277,** 5692–5697
9. Arakawa, R., and Yokoyama, S. (2002) *J. Biol. Chem.* **277,** 22426–22429
10. Wang, N., Chen, W., Linsel-Nitschke, P., Martinez, L. O., Agerholm-Larsen, B., Silver, D. L., and Tall, A. R. (2003) *J. Clin. Investig.* **111,** 99–107
11. Tanaka, A. R., Abe-Dohmae, S., Ohnishi, T., Aoki, R., Morinaga, G., Okuhira, K. I., Ikeda, Y., Kano, F., Matsuo, M., Kioka, N., Amachi, T., Murata, M., Yokoyama, S., and Ueda, K. (2003) *J. Biol. Chem.* **278,** 8815–8819
12. Kameya, S., Miyagoe, Y., Nonaka, I., Ikemoto, T., Endo, M., Hanaoka, K., Nabeshima, Y., and Takeda, S. (1999) *J. Biol. Chem.* **274,** 2193–2200
13. Tanaka, A. R., Ikeda, Y., Abe-Dohmae, S., Arakawa, R., Sadanami, K., Kidera, A., Nakagawa, S., Nagase, T., Aoki, R., Kioka, N., Amachi, T., Yokoyama, S., and Ueda, K. (2001) *Biochem. Biophys. Res. Commun.* **283,** 1019–1025
14. Abe-Dohmae, S., Suzuki, S., Wada, Y., Hiroyuki Aburatani, E. Vance, D., and Yokoyama, S. (2000) *Biochemistry* **39,** 11092–11099
15. Akamatsu, M., Aota, S.-i., Suwa, A., Ueda, K., Amachi, T., Yamada, K. M., Akiyama, S. K., and Kioka, N. (1999) *J. Biol. Chem.* **274,** 35933–35937
16. Gee, S. H., Quenneville, S., Lombardo, C. R., and Chabot, J. (2000) *Biochemistry* **39,** 14638–14646
17. Hamon, Y., Broccardo, C., Chambenoit, O., Luciani, M., Toti, F., Chaslin, S., Freyssinet, J., Devaux, P., McNeish, J., Marguet, D., and Chimini, G. (2000) *Nat. Cell Biol.* **2,** 399–406
18. Fitzgerald, M. L., Mendez, A. J., Moore, K. J., Andersson, L. P., Panjeton, H. A., and Freeman, M. W. (2001) *J. Biol. Chem.* **276,** 15137–15145
19. Remaley, A. T., Stonik, J. A., Demosky, S. J., Neufeld, E. B., Bocharov, A. V., Vishnyakova, T. G., Eggerman, T. L., Patterson, A. P., Duverger, N. J., Santamarina-Fojo, S., and Brewer, H. B., Jr. (2001) *Biochem. Biophys. Res. Commun.* **280,** 818–823
20. Neufeld, E. B., Remaley, A. T., Demosky, S. J., Stonik, J. A., Cooney, A. M., Comly, M., Dwyer, N. K., Zhang, M., Blanchette-Mackie, J., Santamarina-Fojo, S., and Brewer, H. B., Jr. (2001) *J. Biol. Chem.* **276,** 27584–27590
21. Peters, M. F., Adams, M. E., and Froehner, S. C. (1997) *J. Cell Biol.* **138,** 81–93

22. Ort, T., Voronov, S., Guo, J., Zawalich, K., Froehner, S. C., Zawalich, W., and Solimena, M. (2001) *EMBO J.* **20,** 4013–4023
23. Neely, J. D., Amiry-Moghaddam, M., Ottersen, O. P., Froehner, S. C., Agre, P., and Adams, M. E. (2001) *Proc. Natl. Acad. Sci. U. S. A.* **98,** 14108–14113
24. Hua, X., Yokoyama, C., Wu, J., Briggs, M. R., Brown, M. S., Goldstein, J. L., and Wang, X. (1993) *Proc. Natl. Acad. Sci. U. S. A.* **90,** 11603–11607
25. Sato, R., Inoue, J., Kawabe, Y., Kodama, T., Takano, T., and Maeda, M. (1996) *J. Biol. Chem.* **271,** 26461–26464
26. Repa, J. J., and Mangelsdorf, D. J. (2002) *Nat. Med.* **8,** 1243–1248
27. Feng, B., and Tabas, I. (2002) *J. Biol. Chem.* **277,** 43271–43280
28. Kachinsky, A. M., Froehner, S. C., and Milgram, S. L. (1999) *J. Cell Biol.* **145,** 391–402
29. Buechler, C., Boettcher, A., Bared, S. M., Probst, M. C., and Schmitz, G. (2002) *Biochem. Biophys. Res. Commun.* **293,** 759–765
30. Takahashi, Y., and Smith, J. D. (1999) *Proc. Natl. Acad. Sci. U. S. A.* **96,** 11358–11363
31. Fitzgerald, M. L., Morris, A. L., Rhee, J. S., Andersson, L. P., Mendez, A. J., and Freeman, M. W. (2002) *J. Biol. Chem.* **277,** 33178–33187
32. Rigot, V., Hamon, Y., Chambenoit, O., Alibert, M., Duverger, N., and Chimini, G. (2002) *J. Lipid Res.* **43,** 2077–2086

Human Molecular Genetics, 2004, Vol. 13, No. 5 **495–507**
DOI: 10.1093/hmg/ddh056
Advance Access published on January 13, 2004

Muscleblind protein, MBNL1/EXP, binds specifically to CHHG repeats

Yoshihiro Kino, Daisuke Mori, Yoko Oma, Yuya Takeshita, Noboru Sasagawa and Shoichi Ishiura*

Department of Life Sciences, Graduate School of Arts and Sciences, University of Tokyo, 3-8-1 Komaba, Meguro-ku, Tokyo 153-8902, Japan

Received October 13, 2003; Revised and Accepted January 5, 2004

Myotonic dystrophy (DM) type 1 is caused by an expansion of a CTG repeat in the *DMPK* gene and type 2 by a CCTG repeat in the *ZNF9* gene. Previous reports have suggested that transcripts containing expanded CUG/CCUG repeats might have toxic gain-of-function effects, probably affecting the function of RNA-binding proteins in the pathogenesis of DM. Here, it was attempted to compare the RNA-binding properties of three proteins, CUG-BP, MBNL1/EXP and PKR, which have previously been suggested to interact with CUG repeats. MBNL1, but not CUG-BP or PKR, interacted with both CUG and CCUG repeats in a yeast three-hybrid system. By using various synthetic RNAs, it was found that MBNL1 specifically interacts with repetitive sequences summarized as CHHG and CHG repeats, where H is A, U or C. Interestingly, MBNL1 did not interact with a genuine double-stranded RNA comprising CAG/CUG repeats, suggesting that MBNL1 prefers bulge-containing double-stranded RNAs. Deletion analysis indicates a difference in RNA-binding abilities among splice variants of MBNL1. It was also found that MBNL1 can bind to repetitive motifs in *ZNF9*, which contain a minimal length of CCUG repeats with non-CCUG insertions.

INTRODUCTION

Myotonic dystrophy (DM) is an autosomal inherited disorder with multi-systemic and variable symptoms including muscle weakness, myotonia (delayed relaxation of muscle), cataracts, mental retardation and insulin resistance (1). DM can be categorized into two sub-types, DM1 and DM2, according to the kind of mutation. DM1 is caused by an expansion of a CTG repeat located in the 3′ untranslated region (3′-UTR) of the *DM protein kinase* (*DMPK*) gene (19q13.3) (2–4), while DM2 is caused by an expansion of a CCTG repeat located in the first intron of the *ZNF9* gene (3q21) (5). The clinical manifestations of DM1 and DM2 are similar, although there are some differences, such as the presence of a congenital form specific to DM1 (6). Since the *DMPK* and *ZNF9* genes seem to have nothing in common except for the expansion of repetitive sequences, the expansion itself rather than defects in these genes appears to be essential for the pathogenesis of DM. Indeed, no DMPK mutation other than the repeat expansion has ever been reported, suggesting that DM1 is not caused by a loss-of-function of *DMPK* itself. In addition, mice deficient in DMPK show mild myopathy and abnormalities in cardiac conductance, but do not recapitulate other symptoms of DM1 (7–9). On the other hand, transgenic mice with a CUG_{250} repeat expressed in the 3′-UTR of the muscle-specific actin gene show myotonia and progressive myopathy (10), suggesting that the expression of an expanded CUG repeat is sufficient for causing these symptoms independently from the genetic context around DMPK. Since the severity of phenotypes in model mice is related to the expression level of expanded CUG repeats (10), the expanded RNA itself might have toxic effects on cells. Notably, by using fluorescent *in situ* hybridization (FISH) techniques, several investigators have shown that CUG repeat RNAs form nuclear foci in cells or tissues of DM1 patients and DM1 model cells and mice expressing expanded CUG repeats (10–14). Furthermore, expanded CCUG repeat RNAs also form nuclear foci in cells of DM2 (5,14), suggesting that these expanded transcripts have some role in the pathogenesis. One reasonable explanation is that the expanded CUG/CCUG repeat RNA might affect the function of RNA-binding proteins in a *trans*-dominant manner, presumably by their sequestration or aberrant activation, leading to cytotoxic effects. To date, several proteins have been suggested to interact with CUG repeats in *in vitro* or *in vivo* experiments.

One such protein is CUG–binding protein 1 (CUG–BP), first identified as a binding protein for a CUG_8 probe in gel

*To whom correspondence should be addressed. Tel/Fax: +81 354546739; Email: cishiura@mail.ecc.u-tokyo.ac.jp

retardation analysis (15,16). CUG–BP is the first discovered member of the CELF (CUG–BP and ETR3-like factors) proteins and acts as a regulator of alternative splicing (17–20), translation (21,22) and deadenylation (23). Remarkably, several reports have shown the involvement of this protein in the symptoms of DM1, particularly myotonia and insulin resistance, by aberrantly regulating the alternative splicing of chloride channel 1 (CLC-1) and insulin receptor (IR), respectively (19,20). Cardiac troponin T (cTNT) is also a target of CUG–BP, and its splicing pattern is altered in DM1 patients (18). It has also been suggested that a loss of translational induction by CUG–BP in DM1 cells results in the reduction of p21, a key factor in the cell cycle and differentiation, and leads to the defect in myogenic progression (24). Therefore, it is almost certain that CUG–BP is a very important factor in the pathogenesis of DM.

As indicated by its name, the sequestration of CUG–BP by expanded CUG repeats was first assumed. However, whether this protein is actually sequestered by the expanded repeats is controversial, because it does not co-localize with nuclear RNA foci in DM1 or DM2 cells (25,26). The interaction between CUG–BP and CUG repeat RNA is not length-dependent (27). Moreover, contrary to its name, CUG–BP specifically binds to UG motifs rather than to CUG repeats (28), and its binding to CUG repeats seems to be weak (28,29). Nevertheless, a recent paper has shown that CUG–BP binds to an expanded CUG repeat *in vitro* (30), making the situation more complicated. Thus it remains elusive whether CUG–BP actually interacts with CUG/CCUG repeats.

Another group of candidates is the muscleblind protein family, consisting of MBNL1/EXP, MBNL2/MBLL and MBNL3/MBXL/MBLX/CHCR. All these proteins have been shown to co-localize with RNA foci in the cells of both DM1 and DM2 patients, suggesting that they interact with both CUG and CCUG repeats (14,25,26). MBNL1 interacts with CUG repeats in a length-dependent manner (31). In contrast to CUG–BP, however, it is still unclear whether MBNL proteins are involved in the symptoms of DM. Although, *muscleblind*, the fly ortholog of MBNLs, has been reported to play some role in the differentiation of the eye and muscle (32,33), the molecular function and characteristics of MBNL1 are currently unknown.

The third candidate is PKR, a protein kinase activated by double-stranded RNA. Since CUG repeats can form stable double-stranded hairpin structures (34), it is conceivable that CUG repeats are a potential target of PKR. Previous *in vitro* experiments have shown that PKR binds to CUG repeat RNAs in a length-dependent manner and the activation of PKR by CUG repeats has been observed to also be length-dependent (34). Since PKR plays multiple roles in various cellular events such as the anti-viral response, signal transduction, cell growth and apoptosis (35), the abnormal activation of PKR might cause impairments in several cellular functions. However, the involvement of PKR in the pathogenesis of DM is not clear as in the case of MBNL proteins.

To understand the mechanism of DM, the characterization of proteins interacting with CUG/CCUG repeats is important, because this may be related to events downstream of the repeat expansion and its expression. In this study, we tried to reveal the RNA-binding properties of three proteins, CUG–BP, MBNL1 and PKR, to compare their interactions with CUG/CCUG repeats. These proteins have not previously been analyzed together in the same experimental system. We found that MBNL1, but not CUG–BP or PKR, interacts with both CUG and CCUG repeats in an *in vivo* system. Next, we characterized the binding specificity of MBNL1 since its binding target might also be involved in the pathogenesis of DM. For this purpose, we generated an array of repetitive sequences to profile the RNA-binding properties. Our system clearly shows differences in the RNA-binding properties of the above proteins. We determined the target sequence of MBNL1, suggesting that this protein has a novel RNA-binding property.

RESULTS

Comparative analysis of RNA-binding proteins

The RNA-binding proteins assayed in this study are shown in Figure 1A. The isoform of CUG–BP used here does not have an LYLQ insertion (28). $MBNL1_{40}$ is a 40 kDa isoform of MBNL1. A p20 PKR fragment corresponds to its double-stranded RNA binding domain (36,37), and was previously suggested to interact with CUG repeats in a gel retardation assay (34). We used a yeast three-hybrid system, in which the interaction between RNA and protein can be detected by the activity of reporter genes (38,39) (Fig. 1B). Two kinds of assay were performed: an *HIS3* assay and a β-galactosidase (β-gal) assay. In the former assay, yeast transformants are picked up onto a plate lacking histidine, on which *HIS3* activity is necessary for histidine synthesis. The *HIS3* gene product is competitively inhibited by 3-amino-1,2,4-triazole (3-AT) in a dose-dependent manner. Therefore, the expression of *HIS3*, which is activated by the interaction between RNA and protein, can be detected by the viability of yeast transformants on plates containing 3-AT but no histidine. By varying the concentration of 3-AT, the activation can be classified according to the viability of yeast. The β-gal assay is more quantitative in simply measuring the β-gal activity in cell lysates of yeast transformants.

The results of the *HIS3* assay are shown in Table 1. Neither CUG–BP nor PKR interacted strongly with CUG/CCUG repeats, although these proteins are not inactive in yeast (see below). Figure 2A also shows that the activation of β-gal was almost negligible with CUG and CCUG repeats compared with a UG repeat when CUG–BP was used as a prey. As shown in Figure 2C, the activation induced by PKR and CUG/CCUG repeats was also undetectable. By contrast, MBNL1 showed apparent interactions with both CUG and CCUG repeats. This was also confirmed by the β-gal assay as shown in Figure 2B. We could not reproduce the length-dependent interaction between CUG repeats and MBNL1, which preferably interacts with CUG_{21} but not so much with longer repeats. The reasons why MBNL1 preferred CUG_{21} might be attributable to the limitation of the yeast three-hybrid system rather than indicating an actual preference of MBNL1 for CUG_{21}. Since hybrid RNAs are transcribed by RNA polymerase III, which produces relatively small RNAs in general, longer repetitive sequences might not be efficiently transcribed (39). Another possibility is that the GAL4 activation domain fused to RNA-binding proteins that interact with long RNAs might be located at a distance from the promoter region, thus leading to inefficient activation. Taking the principal of this system into

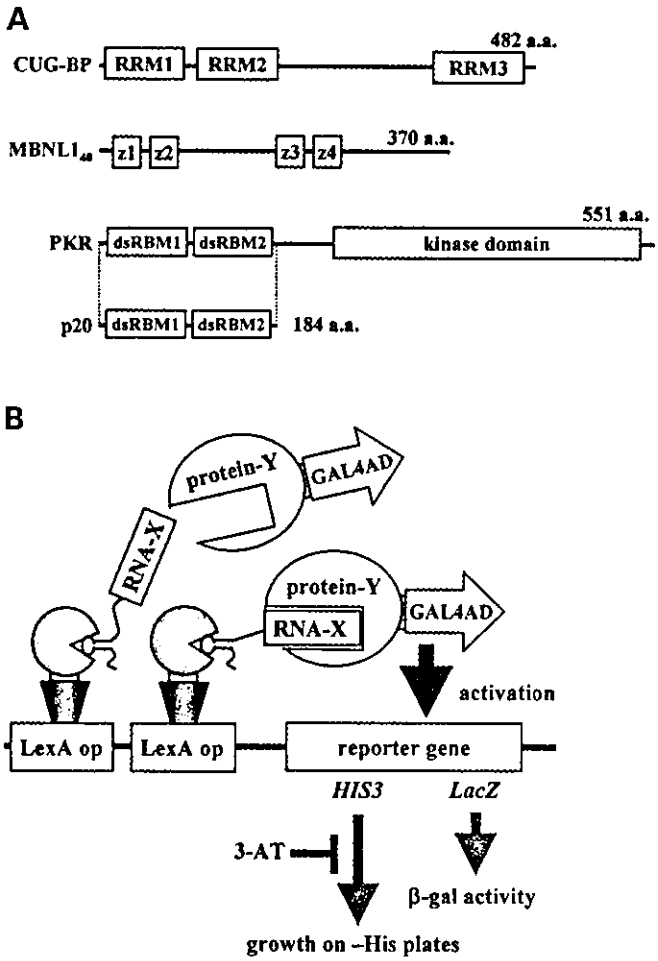

Figure 1. Yeast three-hybrid analysis. (**A**) Structures of the RNA-binding proteins examined in this work. Motifs involved in RNA-binding are indicated by boxes. RRM, RNA recognition motif. z, CCCH-type zinc finger motif. dsRBM, double-stranded RNA binding motif. (**B**) Scheme of the yeast three-hybrid system. Reporter genes (*HIS3* and *LacZ*) downstream of the LexA operator (LexA op) are integrated in the genome of yeast strain *L40-coat*. A fusion protein of LexA and MS2 coat protein (dotted shape) binds to the operator. RNA-X is expressed as a hybrid RNA with MS2 recognition sites, through which the hybrid RNA binds to LexA-MS2 coat fusion protein, and connected to a LexA operator. Protein-Y is expressed as a fusion with GAL4 activation domain (GAL4AD). When RNA-X binds to protein-Y, GAL4AD activates the expression of the reporter genes. Since the gene product of *HIS3*, which is required for cell growth on plates lacking histidine, is competitively inhibited by 3-AT. The concentration of 3-AT at which yeast transformants can grow represents the activity of *HIS3*.

account, it seems natural that there is a threshold length of each RNA for efficient activation, rather than no limitation of RNA length. Nevertheless, the interaction between MBNL1 and CUG/CCUG repeats was obvious and consistent with the results of previous FISH analyses.

Characterization of RNA-binding properties using an array of repetitive sequences

To characterize the binding specificities of the RNA-binding proteins described above, we generated a variety of repetitive sequences, including tri-, tetra- and penta-nucleotide repeats,

Table 1. Results of *HIS3* assay of CUG and CCUG repeats

	CUG-BP	MBNL1	PKR (p20)
MS2-2	–	–	–
UG 24	+++++	–	–
CA 24	–	–	–
CUG 7	–	–	–
CUG 16	–	++	–
CUG 21	–	+++	–
CUG 37	–	++	–
CUG 41	+	++	–
CUG 47	–	++	–
CUG 70	–	++	+
CCUG 7	+	–	–
CCUG 22	–	++++	–
CCUG 50	–	++++	–
CAGG 22	–	–	–
CAGG 50	+	–	–

and examined them in the *HIS3* assay. The results are shown in Table 2. As previously reported (28), CUG-BP interacted strongly with UG-containing sequences such as UG_{12}, UG_{24}, $UCUG_{32}$ and $UAUG_7$. It also interacted with a UCCG repeat, suggesting that CUG-BP prefers GU motifs as well as UG motifs. Although both $CCUG_{22}$ and $CUGG_{50}$ repeats contain UG motifs, CUG-BP did not interact with them. This might be due to their secondary or higher structures.

PKR strongly interacted with $UAUG_7$+$CAUA_7$, CUG_{16}+CAG_{16} and $CCUG_{22}$+$CAGG_{22}$ repeats, which might form double-stranded hairpins. Although we have no direct evidence for the structures of these RNAs in cells, it seems natural that they are dsRNA in cells. Indeed, CUG-BP did not interact with $UAUG_7$+$CAUA_7$, although it interacted preferentially with the UAUG repeat alone, suggesting that the former sequence might have a different structure from the latter. Interestingly, PKR interacted with CAG repeats to some extent, consistent with a previous report in which PKR bound to transcripts of huntingtin with expanded CAG repeats (40). This might be because CAG repeat can form double-stranded structures containing bulges (mispairs). Surprisingly, PKR did not interact with CUG repeat, although this RNA can be expected to have a structure similar to CAG repeats.

MBNL1 interacted strongly with $CCCG_{21}$, modestly with $CUUG_{38}$ and $CAAG_{38}$, weakly with $CCAG_{50}$, CAG repeats, CCG_{30}, and $CAUG_7$, but not at all with $CGGG_{20}$, $CUGG_{50}$, and CAGG repeats. The deduced consensus MBNL1 binding sequence is CHHG or CHG, where H corresponds to A, C or U (not G). Importantly, both of these sequences form double-stranded structures with bulges. Interestingly, MBNL1 did not interact with CUG_{16}+CAG_{16} or $CCUG_{22}$+$CAGG_{22}$, with which PKR interacted strongly. This indicates that MBNL1 seems to prefer double-stranded RNAs containing bulges. Unlike CUG-BP, which can bind to both UG and GU motifs, MBNL1 did not interact with the UCCG repeat, the reverse (but not complementary) sequence of the CCUG repeat. UCCG appears to form a double-stranded structure, but not suitable for the consensus of CHHG, suggesting that there is some kind of sequence selectivity in the recognition by MBNL1. Alternatively, UCCG does not have a hairpin structure in the cell, as CUG-BP interacted well with this sequence. We have examined several pentanucleotide repeats, some of which

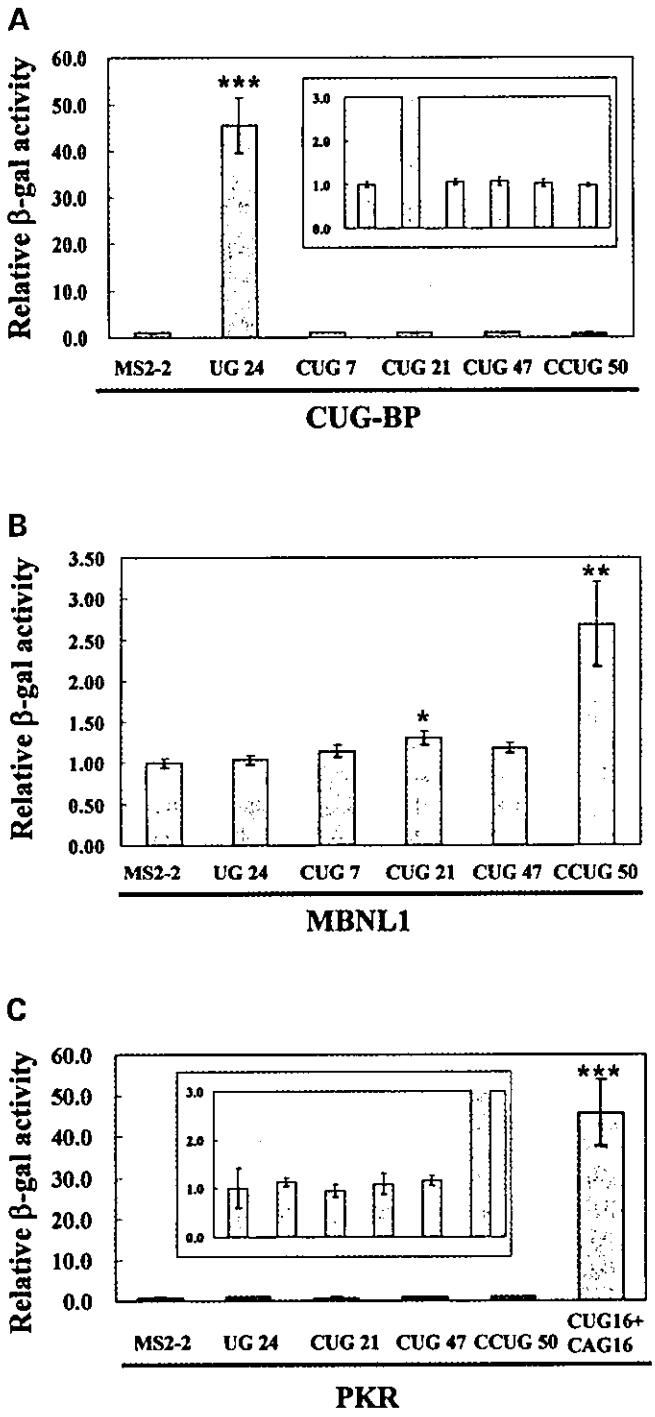

Figure 2. Results of β-galactosidase assay. Bars represent the average value of relative β-galactosidase activities of four independent transformants. The RNA sequences used are shown below the bars. Error bars correspond to standard deviations. MS2-2 is a negative control with no repetitive insertion. Insets shows the same bars with magnified scales. (**A**) Results of the interaction of CUG–BP with repetitive RNAs. The β-galactosidase activity is very strong with UG repeats, while it is almost not detectable with CUG and CCUG repeats. (**B**) Results with MBNL1. A relatively strong activation was observed with $CCUG_{50}$ and a small amount activation was observed with CUG_{21}. (**C**) Results with PKR. An intense activation was observed with CUG_{16}+CAG_{16}, while no detectable activation was observed with other RNAs. Significant difference from MS2-2: $^{***}P < 0.001$, $^{**}P < 0.01$, $^{*}P < 0.05$, in one-way ANOVA, followed by Tukey type multiple comparison.

Table 2. RNA-binding specificities of CUG–BP, MBNL1 and PKR in *HIS3* assay

	CUG–BP	MBNL1	PKR (p20)
UA 30	−	−	+++
CAG 16	−	++	++
CAG 41	+	++	++
CAG 70	−	++	++
CCG 30	++	++	−
CGG 30	+	−	−
AAG 30	−	−	−
CCU 37	−	−	−
UCUG 32	++++	−	+
CAGA 32	++	−	+
UCCG 27	++++	−	+
CGGA 30	++	−	+
CUGG 50	−	−	−
CCAG 50	−	++	−
CAAG 38	−	+++	−
CUUG 38	+	+++	−
CGGG 20	−	−	−
CCCG 21	++	++++	−
UAUG 7	+++	−	−
CAUA 7	−	−	−
CAUG 7	++	++	++
CUGAG 19	−	−	++++
CUCAG 19	−	−	++
CCUAG 13	−	+	−
CUAGG 13	−	−	+
CAUUG 16	−	−	+
CAAUG 16	−	−	+++
UAUG7+CAUA7	−	−	+++++
CUG16+CAG16	−	−	+++++
CCUG22+CAGG22	−	−	+++++

presumably form bulge-containing double-stranded structures. Although PKR interacted with some of them, for example, $CUGAG_{19}$ and $CAAUG_{16}$, MBNL1 showed almost no interaction with any of these sequences. Together with the observation that MBNL1 seems to prefer tetranucleotide repeats over trinucleotide repeats, these results suggest that the number of nucleotides in each repetitive unit and/or the ratio of bulges in the duplex might also be important for the binding of MBNL1.

At last, two points should be noted about three-hybrid assays. First, the strength of maximum reporter activity is varied among proteins, since fusing them with GAL4 activation domain might affect their RNA-binding activity and/or transcriptional activity. This effect may depend on the structure of each proteins. Therefore, it is not strange that the maximum activities of each protein (i.e. CUG–BP–UG_{24}, PKR–CUG_{16}+CAG_{16} and MBNL1–$CCUG_{50}$) differ largely. However, it is also possible that some unknown sequences show higher reporter activities than CCUG repeats in combination with MBNL1. Next, these large differences in β-gal assay do not appear to be reproduced in the *HIS3* assays shown in Tables 1 and 2, in which CUG–BP–UG_{24} and PKR–CUG_{16} + CAG_{16} were classified as (+++++), while MBNL1 was (++++). We examined the former two combinations on the selection plates containing much higher concentration of 3-AT than 1 mM, resulting in the growth of these transformants in the presence of at least 10 mM 3-AT (data not shown). Therefore, the tendencies of reporter activities in these two assays do not seem to be considerably different.

Deletion analysis of MBNL1

MBNL1 has at least nine splice variants, which we tentatively name here as shown in Figure 3B. Seven of them, $MBNL1_{42}$, $MBNL1_{41}$, $MBNL1_{40}$, $MBNL1_{41s}$, $MBNL1_{40s}$, $MBNL1_{36}$ and $MBNL1_{35}$, have been reported previously (25,31), while $MBNL1_n$ and MBNL1 delta N ($MBNL1_{\Delta N}$) are novel isoforms. The existence of the latter two is suggested by ESTs, AL562860 (and others) and BC050535, respectively. $MBNL1_n$ is an isoform containing only the N-terminus short region of MBNL1 with a single zinc finger motif. This isoform has a distinct C-terminus and 3′-UTR from other isoforms. On the other hand, $MBNL1_{\Delta N}$ lacks the N-terminus region and starts in the second zinc finger motif, resulting in the loss of this motif. Thus, this isoform has only two intact zinc finger motifs out of four. Since MBNL1 has a variety of C-terminus regions, $MBNL1_{\Delta N}$ also has more splice variation in the C-terminus other than as shown in Figure 3B.

To determine the contribution of each zinc finger motif to RNA-binding, deletion analysis of MBNL1 was performed using a yeast three-hybrid system. We generated 10 deletion constructs (del 1–10) as shown in Figure 3C, and their affinities for $CCUG_{22}$ and CUG_{21} are indicated. Del 1 has a deletion in the C-terminus and corresponds to the maximum common region among $MBNL1_{42}$, $MBNL1_{41}$, $MBNL1_{40}$, $MBNL1_{41s}$ and $MBNL1_{40s}$. Del 2 lacks the alanine-rich region in the C-terminus of del 1. Del 3–6 are deletion constructs with various zinc finger motifs. Del 7–9 lack a region (amino acids 116–183) that is also missing from $MBNL1_{36}$ and $MBNL1_{35}$. Del 10 mimics the deletion of the N-terminus, $MBNL1_{\Delta N}$. As can be seen in Figure 3C, deletions of the C-terminus and flanking alanine-rich region cause no reduction in the RNA binding activity in *HIS3* assay (del 1 and del 2, respectively). Rather, these two mutants appear to have increased binding activity, probably because of the structural facilitation of RNA binding or the activation of the reporter gene due to the lack of the C-terminus region. The deletions of each zinc finger motif suggest that all four zinc fingers are necessary for full RNA-binding ability, although the deletion of the fourth zinc finger (del 6) still allowed some binding to $CCUG_{22}$. Interestingly, del 7, which has all four zinc fingers, lost most of its binding abilities, suggesting that the linker region between the second and third zinc fingers is also needed for binding to the CCUG/CUG repeats, or that this long linker is necessary for the structural integrity of MBNL1. As del 1 and del 2 correspond to the common region among $MBNL1_{42}$, $MBNL1_{41}$, $MBNL1_{41s}$, $MBNL1_{40}$ and $MBNL1_{40s}$, these splice isoforms might interact with CCUG and CUG repeats. On the other hand, other variants, $MBNL1_{36}$, $MBNL1_{35}$, $MBNL1_{\Delta N}$ and $MBNL1_n$, might not interact with these repeats, since they lack either zinc fingers or the linker region necessary for the binding. If this is the case, there might be a difference among MBNL1 isoforms in their interactions with expanded repeats.

In vitro binding experiments of GST-MBNL1

To confirm the results of the three-hybrid analyses, we performed gel retardation analysis. First, we fused $MBNL1_{40}$ with glutathione *S*-transferase (GST) in the N-terminus and a Histidine-tag (His-tag) in the C-terminus (GST–MBNL1) (Fig. 4A). GST–MBNL1 was expressed in *E. coli* and purified by affinity chromatography. Gel retardation analysis suggested that GST–MBNL1 bound to a ^{32}P-labeled $CCUG_{15}$ probe (Fig. 4B, lane 3), and supershift was observed when an anti-GST antibody was added (Fig. 4B, lane 5). The extent of band shift was reduced by adding non-labeled $CCUG_{15}$ RNA (Fig. 4B, lane 4), suggesting the specificity of the binding. Figure 4C shows the effects of ion concentration. The formation of the RNA–protein complex was disrupted at higher concentrations of KCl and NaCl (Fig. 4C, lanes 9–11 and 15–17). The complex of GST–MBNL1 and $CCUG_{15}$ was subjected to RNase V1 treatment. RNase V1 specifically cleaves base-paired nucleotides. Figure 4D shows the partial protection of $CCUG_{15}$ from cleavage in the presence of GST–MBNL1 (lanes 20 and 23), further confirming the binding.

Next, we confirmed that GST–MBNL1 can bind to CUUG, CCCG and CAAG repeats, but not with CAGG and CGGG repeats (Fig. 5, left), consistent with the results of the yeast system. GST–MBNL1 also interacted with CUG repeats but not with CAG repeats, a finding not consistent with the yeast three-hybrid system. Similar results were reported in the previous study using the UV crosslink method (31). Since this discrepancy may reflect the difference in experimental systems, it is unclear whether MBNL1 actually binds to CAG repeats. Mostly consistent with the results of the yeast system, GST–MBNL1 interacted with CCUG repeats more specifically than with the other CHHG repeats, since the binding to CCUG could be detected with a much smaller amount of MBNL1 (Fig. 5, top right). We also examined the *in vitro* binding of GST–CUG–BP, but the binding to CUG and CCUG repeats was nearly undetectable at the level of GST–CUG–BP used in Figure 5 (right bottom).

We also examined the dependence of the binding between CCUG repeats and MBNL1 on the repeat length. As shown in Figure 6A, free probes of $CCUG_{27}$ and $CCUG_{35}$ disappeared at the highest dose of MBNL1, while that of $CCUG_{15}$ remained unbound at the same dose of GST–MBNL1 (lanes 4, 8 and 12). This might reflect the length-dependent formation of a particular structure that is recognized by GST–MBNL1. In this assay, the number of shifted bands represents the variety of RNA–protein complexes, mainly reflecting the number of proteins binding to a single probe. There were two bands of RNA–protein complexes with $CCUG_{15}$ (Fig. 6A, lane 4), while at least four kinds of band could be seen with $CCUG_{27}$ and $CCUG_{35}$ (Fig. 6A, lanes 6–8 and 10–12), indicating that a larger numbers of GST–MBNL1 proteins bind to CCUG probes as the RNA grows longer. These results show the length-dependent binding of MBNL1, probably accompanied by the transition of the RNA structure, and an increase in the number of binding sites for GST–MBNL1. Longer repeats were also examined by competition analysis (Fig. 6B). Consistent with Figure 6A, $CCUG_{35}$ showed more preferential binding to MBNL1 than $CCUG_{15}$, confirmed by its efficient competition (lanes 15 and 18, or 16 and 19). Moreover, $CCUG_{120}$ fully competed to the labeled probe at the lowest dose, while $CCUG_{35}$ left a bandshift at the same dose (lane 17, see also lane 20), suggesting that $CCUG_{120}$ has higher affinity to MBNL1 than $CCUG_{35}$. Consistent with the results of Figure 5, competition by CUG repeats was less evident than that by CCUG repeats (Fig. 6B, bottom). However, at the highest dose,

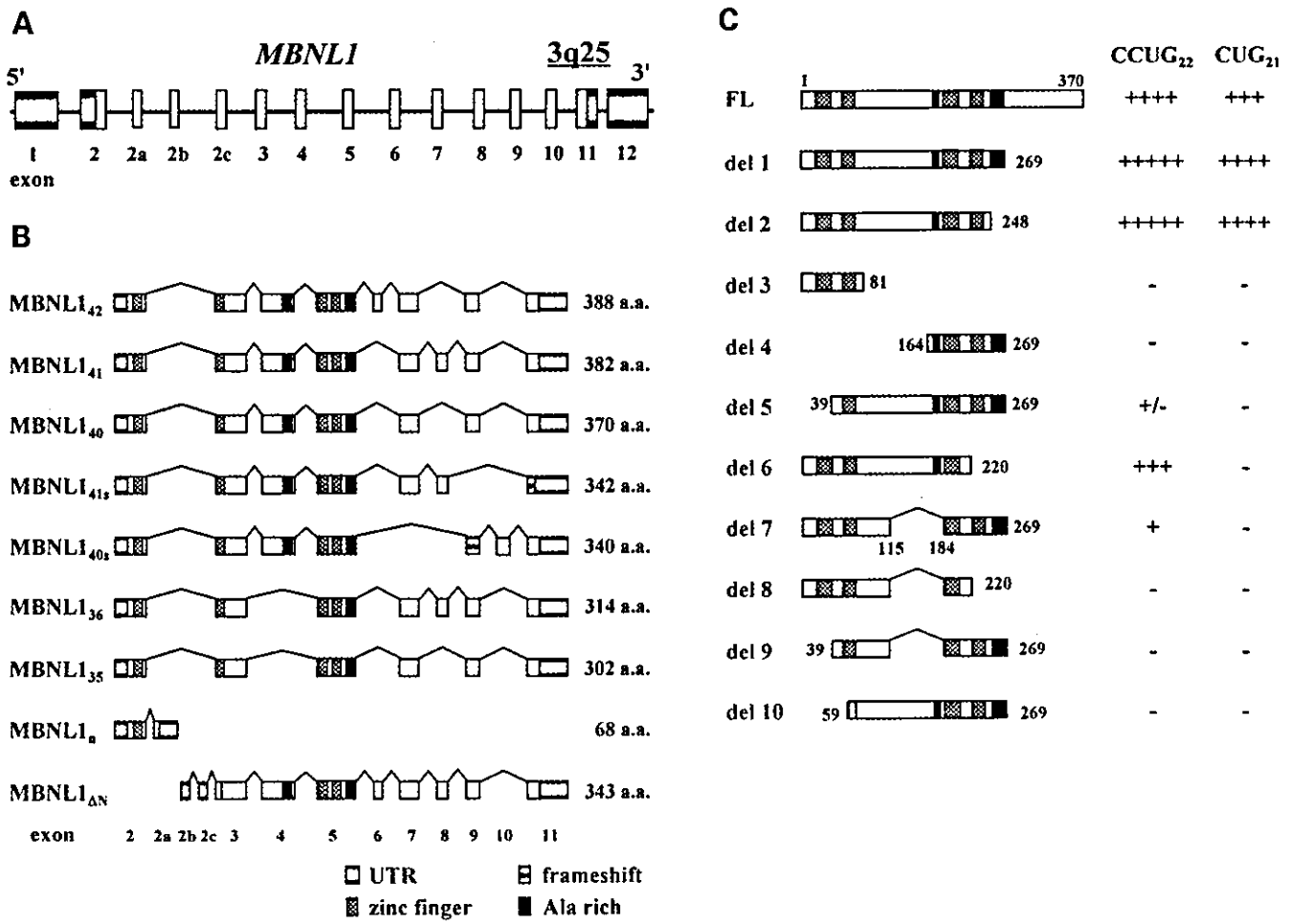

Figure 3. Splice variants and deletion analysis of MBNL1. Exons of *MBNL1* are represented as boxes. Note that the length of each box does not reflect the actual genomic structure of *MBNL1*. (**A**) Order and name of exons used in this work. (**B**) Open reading frames of each variant are indicated by open boxes. Other boxes corresponding to UTR, zinc finger motifs and alanine-rich regions are indicated in the bottom. MBNL1$_n$ and MBNL1$_{\Delta N}$ are novel isoforms. The zinc finger motif in exon3 of MBNL1$_{\Delta N}$ is disrupted since it requires a cysteine in exon 2. Striped boxes represent frameshift of some isoforms compared to the corresponding exons of other isoforms. (**C**) Full-length MBNL1$_{40}$ (FL) and its deletion mutants (del 1–10) were examined in the yeast three-hybrid system (*HIS3* assay) with CCUG$_{22}$ and CUG$_{21}$ hybrid RNAs. Numbers indicate the amino acid composition of each variant. Amino acids 116–183, deleted in del 7–del 9, correspond to the region deleted in MBNL1$_{35}$ and MBNL1$_{36}$. Results of HIS3 assay are indicated at the right with the same code as in Tables 1 and 2. Zinc finger motifs and alanine-rich regions are indicated as the same boxes in (B).

only CUG$_{130}$ showed apparent competition (lane 32), suggesting that MBNL1 prefers longer CUG repeats, which is in agreement with the previous finding using UV-crosslink method (31). Importantly, since we used the same doses (nanograms) of competitor RNAs, longer CUG/CCUG repeats should have fewer molecules than shorter repeats. Therefore, the preferential binding of MBNL1 to longer CUG/CCUG suggests that these RNAs sequester larger number of MBNL1 molecules per a single RNA than shorter ones.

The above results and those of previous studies apparently show MBNL1 to be a repeat RNA-binding protein. To examine whether MBNL1 binds to DNA, competition analysis was performed. Several unlabeled single-stranded oligo DNAs were used as cold competitors. Figure 7A shows that CCTG$_{22}$ competed with the binding of GST–MBNL1 to CUG$_{41}$ (lane 4), suggesting that MBNL1 can interact with DNA as well as RNA. Since other DNAs did not compete as efficiently as CCTG, MBNL1 might have a similar sequence specificity for DNA to that for RNA. To determine whether MBNL1 prefers RNA or DNA, the competitive efficiencies of cold CCUG$_{15}$ and CCTG$_{22}$ were compared. As shown in Figure 7B, CCUG$_{15}$ competed more efficiently than the CCTG$_{22}$ repeat, suggesting that MBNL1 favors repetitive RNA sequences for binding. Although the lengths of the CCUG and CCTG repeats used here were not the same, we can expect that CCUG$_{22}$ would be a more effective competitor than CCUG$_{15}$, because MBNL1 prefers longer CCUG repeats as suggested above. In this case, the difference in binding specificity between CCUG$_{22}$ and CCTG$_{22}$ might be more prominent than in the case of CCUG$_{15}$ and CCUG$_{22}$. The preference of MBNL1 for RNA rather than DNA may suggest its major role in RNA metabolism.

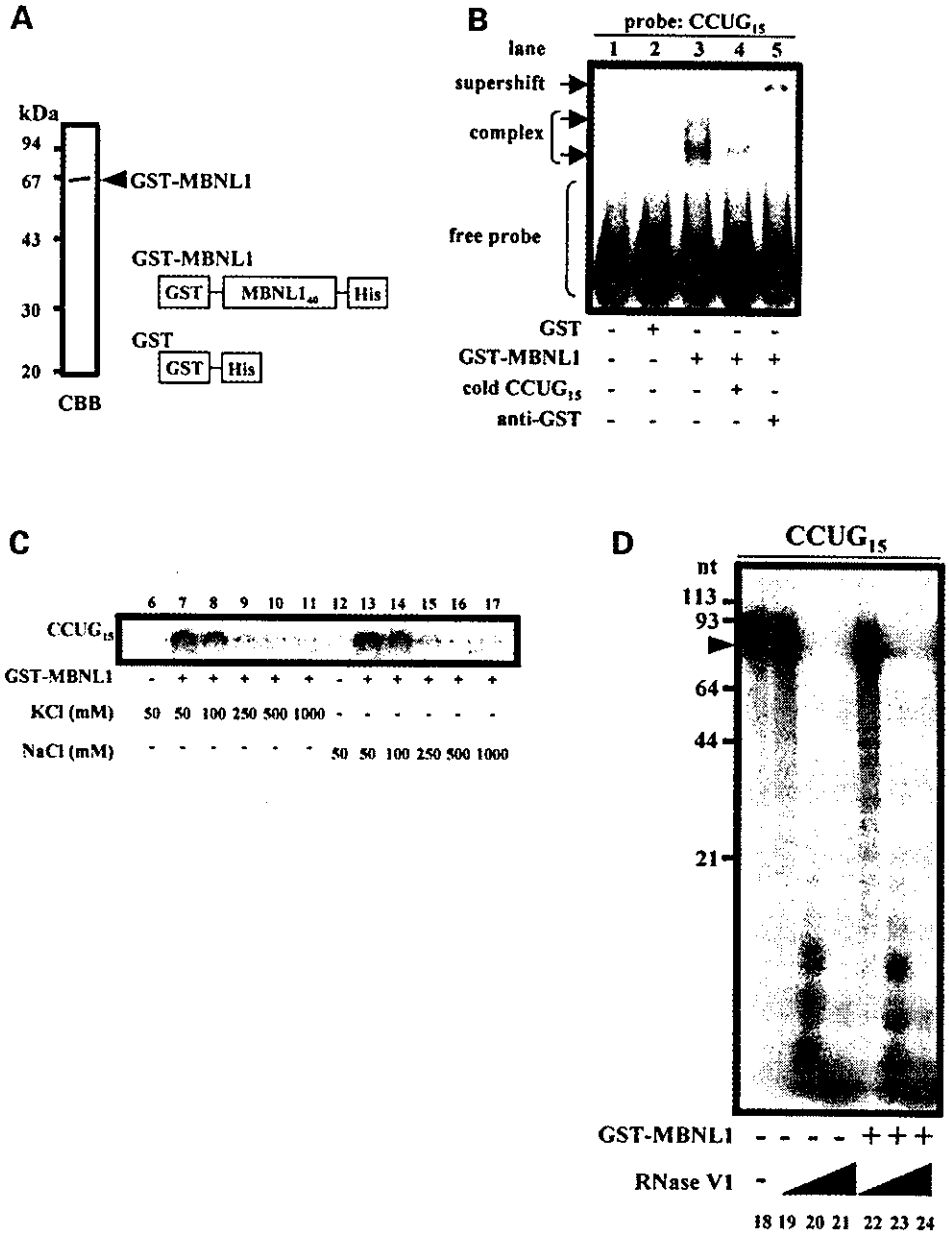

Figure 4. *In vitro* binding of recombinant GST–MBNL1 to CCUG$_{15}$. **(A)** Right, the structures of the GST–MBNL1 and GST recombinant proteins. Both proteins were also tagged with 6× histidine in the C-terminus to facilitate purification. Left, purified GST–MBNL1 stained with CBB. **(B)** Gel retardation analysis of GST–MBNL1 and ^{32}P-labeled CCUG$_{15}$ probe by non-denaturing 5% PAGE. The presence of GST–MBNL1/CCUG$_{15}$ complexes is indicated by arrowheads (lanes 3–5). The addition of non-labeled CCUG$_{15}$ RNA (400 ng) reduced the formation of the shifted band (lane 4). The addition of anti-GST antibody resulted in a supershift of the complex (lane 5). **(C)** The effect of ion concentration. RNA–protein complexes are shown in the panel. Increasing concentrations of KCl (lanes 6–11) or NaCl (lanes 12–17) were added prior to the reaction of GST–MBNL1 and CCUG$_{15}$. Higher concentrations of these salts inhibit binding (lanes 9–11 and 15–17). **(D)** Effect of RNase treatment on the RNA–protein complex. Digestion of the CCUG$_{15}$ probe was analyzed by denaturing 13% PAGE containing 8 M urea. Increasing amounts of RNase V1 (lanes 19 and 22, 0.0001 unit; lanes 20 and 23, 0.001 unit; lanes 21 and 24, 0.01 unit) were added in the presence or absence of GST–MBNL1. The arrowhead shows the original length of the CCUG$_{15}$ probe (83 nt). By comparing lane 20 with lane 23, partial protection of RNA degradation can be observed.

MBNL1 interacts with CCUG repeats in *ZNF9* with minimal lengths

Previous reports have suggested that MBNL1 and its homologs colocalize with expanded CCUG repeats in DM2 (14,26). The length of the CCUG/CCTG repeat is highly polymorphic, ranging from 11 to 26 in normal individuals and from about 75 to several thousand in patients (5,6). To address whether MBNL1 interacts with unexpanded CCUG repeats, we examined the minimal length of CCUG motifs previously reported as shown in Figure 8B (DM2-1 and DM2-2) (5). Both motifs have insertions of non-CCUG tetranucleotides, such as UCUG and GCUG. In the gel retardation assay, GST–MBNL1 interacted specifically with both DM2-1 and DM2-2 (Fig. 8C).

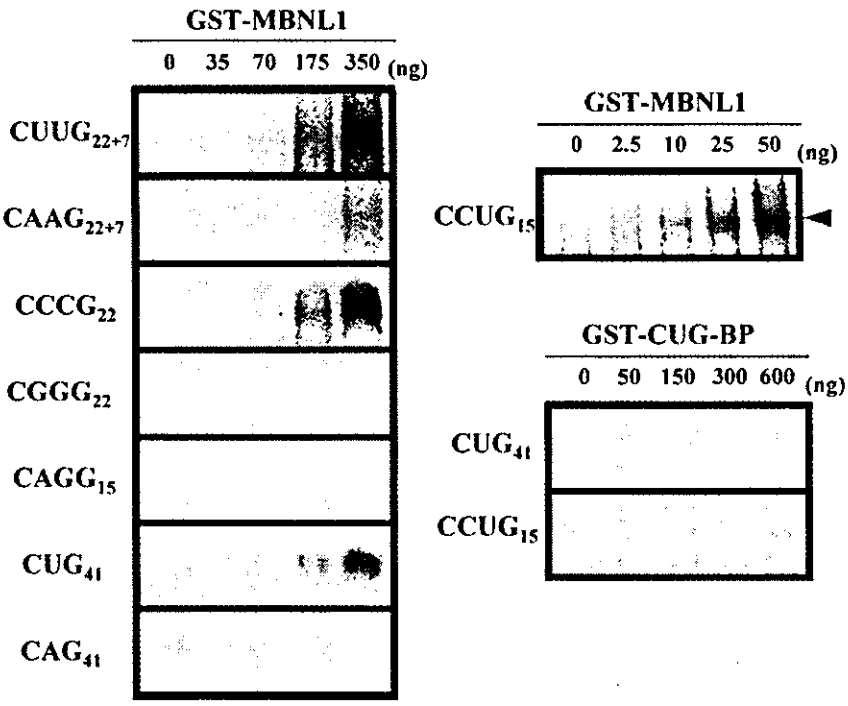

Figure 5. Dose-dependent and sequence-specific binding of GST–MBNL1. Dose-dependent binding of GST–MBNL1 to various repetitive RNA probes was analyzed by gel retardation analysis. ^{32}P-labeled probes as indicated were examined with increasing doses of GST–MBNL1 (left and right top panels). GST–CUG–BP was also analyzed for comparison (right below panel). RNA–protein complexes are shown in each panel.

From this result, we can predict two possibilities. One is that MBNL1 can bind to CCUG repeats despite the presence of the non-CCUG sequences. The other is that MBNL1 might interact with any length of CCUG repeat in human *ZNF9*, because it bound to the minimal CCUG repeat, and it might interact with longer CCUG repeats due to the length-dependence of the binding property.

DISCUSSION

We compared the specificity of three RNA-binding proteins, which were formerly suggested to interact with CUG repeat at least *in vitro*. However, two of them, CUG–BP and PKR, failed to reproduce its interaction with CUG repeats in the yeast three-hybrid system. These proteins also showed little interaction with CCUG repeats. On the other hand, MBNL1 interacted with both CUG and CCUG repeats in this system. In summary, our results indicates that double-stranded structure formed by CUG and CCUG repeats are recognized by MBNL1, but not by CUG–BP or PKR. These results for MBNL1 and CUG–BP in the yeast system are plainly consistent with the previous findings obtained by FISH (14,25,26), probably because both are *in vivo* systems. Evidence, including our present study, suggests that CUG–BP interacts with UG/GU containing single-stranded RNAs and this protein is not suitable for the direct target of the sequestration by the expanded CUG/CCUG RNAs, even though this protein is involved in the abnormal splicing in DM. There has been no report of FISH experiments on PKR or the activation of PKR *in vivo*. If our results actually reflect the *in vivo* function, PKR does not seem to be stably recruited by CUG or CCUG repeats, as in the case of CUG–BP. Yet the possibility of PKR activation by expanded RNAs cannot be ruled out, because an undetectable level of binding might cause its activation and affect cellular functions.

Toxic RNA effects and RNA-binding proteins

To date, RNA gain-of-function in DM has been suggested to have at least two types of cellular effects. Evidence has shown that abnormal splicing is involved in causing some of the symptoms of DM (18–20,41). In addition to CLC-1, IR and cTNT, the altered splicing of tau and myotubularin-related protein 1 has been reported in DM1 (42–44). Aberrant splicing of CLC-1 is also reported in DM2 (41), suggesting that the abnormal splicing event is a significant feature in the pathogenesis of both DM1 and DM2. Since the ectopic expression of the expanded repeat RNA can recapitulate the abnormal splicing patterns in cultured cells and transgenic mice (18,19,41), it is apparent that this phenotype is one of the results of RNA-gain-of-function.

Notably, abnormal splicing is accompanied by the up-regulation of CUG–BP in DM1 tissues and model cells (19,20). Moreover, the overexpression of CUG–BP alone can induce abnormal splicing patterns without the expression of expanded repeats in normal cells (19). Importantly, these indicate that aberrant splicing is induced by the increased activity of CUG–BP, but not by the loss-of-function of this protein. From this point of view, the absence of interaction between CUG–BP and CUG/CCUG repeats shown above and in the FISH analyses is compatible with the role of CUG–BP in